

---

# GRAPHMASTER: AUTOMATED GRAPH SYNTHESIS VIA LLM AGENTS IN DATA-LIMITED ENVIRONMENTS

---

A PREPRINT

 **Enjun Du**

Department of Cyberspace Science and Technology  
Beijing Institute of Technology  
Beijing 100081, China  
EnjunDu.cs@gmail.com

**Xunkai Li**

Department of Computer Science and Technology  
Beijing Institute of Technology  
Beijing 100081, China  
cs.xunkai.li@gmail.com

**Tian Jin**

Pittsburgh Institute  
Sichuan University  
Chengdu 610207 China  
2022141520260@stu.scu.edu.cn

**Zhihan Zhang**

Department of Computer Science and Technology  
Beijing Institute of Technology  
Beijing 100081, China  
3220241443@bit.edu.cn

 **Rong-Hua Li\***

Department of Computer Science and Technology  
Beijing Institute of Technology  
Beijing 100081, China  
lironghuabit@126.com

**Guoren Wang**

Department of Computer Science and Technology  
Beijing Institute of Technology  
Beijing 100081, China  
wanggrbit@gmail.com

April 2, 2025

## ABSTRACT

The era of foundation models has revolutionized AI research, yet Graph Foundation Models (GFMs) remain constrained by the scarcity of large-scale graph corpora. Traditional graph data synthesis techniques primarily focus on simplistic structural operations, lacking the capacity to generate semantically rich nodes with meaningful textual attributes—a critical limitation for real-world applications. While large language models (LLMs) demonstrate exceptional text generation capabilities, their direct application to graph synthesis is impeded by context window limitations, hallucination phenomena, and structural consistency challenges. To address these issues, we introduce **GraphMaster**—the first multi-agent framework specifically designed for graph data synthesis in data-limited environments. GraphMaster orchestrates four specialized LLM agents (Manager, Perception, Enhancement, and Evaluation) that collaboratively optimize the synthesis process through iterative refinement, ensuring both semantic coherence and structural integrity. To rigorously evaluate our approach, we create new data-limited “Sub” variants of six standard graph benchmarks, specifically designed to test synthesis capabilities under realistic constraints. Additionally, we develop a novel interpretability assessment framework that combines human evaluation with a principled Grassmannian manifold-based analysis, providing both qualitative and quantitative measures of semantic coherence. Experimental results demonstrate that GraphMaster significantly outperforms traditional synthesis methods across multiple datasets, establishing a strong foundation for advancing GFMs in data-scarce environments.

---

\*Corresponding author.

# 1 Introduction

In the era of foundation models, unprecedented advances in natural language processing and computer vision have been enabled by massive training corpora [2, 7]. Graph Foundation Models (GFMs) [23, 20] represent a promising frontier for AI in graph-structured data, yet their development faces a critical bottleneck: the scarcity of large-scale, diverse graph datasets. Unlike text and image domains where data collection is relatively straightforward, gathering and annotating graph data often requires specialized expertise and significant resources. This data quantity constraint has become the primary challenge for training robust GFMs, particularly as model size increases and demands exponentially more training examples for optimal performance.

Graph data synthesis offers a strategic solution to this fundamental constraint by automatically generating new graph samples that maintain both semantic richness and structural validity. Existing synthesis approaches, however, face substantial limitations. Edge-level operations [41, 43] manipulate existing connections but cannot create novel nodes or patterns. Node-level mixing techniques like GraphMixup [38] generate synthetic nodes by interpolating features but often produce semantically inconsistent attributes, particularly with textual features. Graph-level synthesis methods such as G-Mixup [14] create entirely new graphs but struggle to balance global structure with local semantic coherence. The core limitation across these traditional methods is their inability to simultaneously preserve meaningful semantics while generating structurally valid expansions—a deficiency particularly pronounced when handling text-attributed graphs (TAGs) where both connectivity patterns and textual node features must remain coherent.

Large language models have demonstrated remarkable capabilities in understanding and generating text [15, 9], suggesting potential for synthesizing text-attributed graphs. However, directly applying LLMs encounters several critical challenges: standard context windows cannot process entire graphs with numerous textual nodes [3]; LLMs excel at semantic understanding but struggle to maintain structural consistency [10]; and without proper coordination, they tend to produce inconsistent or hallucinated content that fails to capture the intricate balance between topology and semantics [25]. Furthermore, in realistic scenarios with limited available data, LLMs have insufficient examples to learn complex graph patterns [19].

To address these challenges, we propose **GraphMaster**, a novel multi-agent framework specifically designed for graph synthesis in data-limited environments. GraphMaster decomposes the complex synthesis task into specialized sub-tasks handled by four collaborative LLM-powered agents, each targeting specific challenges: (1) The Manager Agent coordinates the overall process and determines optimal synthesis strategies based on current graph characteristics, orchestrating the complex synthesis workflow; (2) The Perception Agent analyzes graph structure and employs advanced sampling to identify representative subgraphs processable within LLM context constraints, directly addressing the context window limitations; (3) The Enhancement Agent generates new nodes and edges with consistent semantics and structure, mitigating hallucination by maintaining coherence with existing graph elements; and (4) The Evaluation Agent assesses quality based on both semantic coherence and structural integrity, providing feedback for iterative improvement to ensure structural and semantic consistency. This decomposition enables targeted solutions for each challenge that a single-pass LLM approach cannot address.

Through this collaborative, iterative process, these specialized agents overcome the limitations of both traditional methods and direct LLM applications. The multi-agent architecture enables GraphMaster to effectively balance semantic richness with structural validity—producing high-quality synthetic graph data even with limited training examples. By introducing modular reasoning (through task decomposition), semantic control (via specialized agent expertise), and iterative optimization (through feedback cycles), GraphMaster achieves synthesis capabilities beyond what single-pass approaches can deliver.

Our contributions can be summarized as follows: (1) **New perspective for LLM-based TAG Synthesis**: we first propose a novel multi-agent framework from the RAG perspective to synthesize TAG under data-limited environment. By integrating context retrieval with iterative feedback, this new perspective enables both semantic richness and structural fidelity. (2) **Groundbreaking Benchmark**: We introduce a standardized “Data-limited” variant testbed for text-attributed graph synthesis and develop a dual-perspective interpretability assessment—combining expert human evaluation with Grassmann manifold-based analysis—to provide reproducible comparisons and deep semantic-structural insights. (3) **State-of-the-Art Performance**: Extensive experiments on multiple datasets and GNN architectures demonstrate that our method consistently outperforms existing baselines, setting a new benchmark for data-limited TAG synthesis.

## 2 Background Methods

### 2.1 Classic Graph Data Synthesis Methods

Traditional graph data synthesis methods [6] address data scarcity through various approaches. Edge-level operations [41] modify topology by adding or deleting connections. Node-level techniques like GraphSMOTE [40] generate

new nodes through minority class interpolation. Graph-level methods such as G-Mixup [14] create entirely new graph instances via graphon interpolation. Interpolation-based approaches [32, 31] combine hidden representations to enhance model robustness. Despite their diversity, these methods primarily focus on structural manipulations without generating semantically meaningful textual attributes.

## 2.2 LLM-based Multi-Agent Systems for Data Generation

Recent LLM-powered multi-agent frameworks demonstrate capabilities for complex data generation tasks. General collaboration systems like Self-Instruct [33] and distributed simulation platforms [26] establish architectures for coordinated AI systems. In graph contexts, approaches like GoG [36] and LLM-based social simulations [16] leverage semantic understanding for graph-related tasks. However, specific applications for text-attributed graph synthesis in data-limited environments remain largely unexplored.

## 2.3 Problem Formulation: Graph Data Synthesis

**Text-Attributed Graphs.** We formally define a text-attributed graph (TAG) as  $\mathcal{G} = (\mathcal{V}, \mathcal{E}, \mathcal{X}, \mathcal{Y})$ , where  $\mathcal{V} = \{v_1, v_2, \dots, v_N\}$  is a set of  $N$  nodes,  $\mathcal{E} \subseteq \mathcal{V} \times \mathcal{V}$  is the set of edges with corresponding adjacency matrix  $\mathcal{A} \in \{0, 1\}^{N \times N}$ ,  $\mathcal{X} = \{x_1, x_2, \dots, x_N\}$  is the set of textual features with each  $x_i$  corresponding to node  $v_i \in \mathcal{V}$ , and  $\mathcal{Y} = \{y_1, y_2, \dots, y_N\}$  represents the set of node labels where  $y_i \in \{1, 2, \dots, C\}$  for  $C$  distinct classes.

**Knowledge Extraction.** Given the context length constraints of LLMs, we define a knowledge extraction function  $\Phi : \mathcal{G} \rightarrow \mathcal{K}$  that samples a representative subgraph as:

$$\mathcal{K} = \Phi(\mathcal{G}) = (\mathcal{V}_k, \mathcal{E}_k, \mathcal{X}_k, \mathcal{Y}_k), \quad (1)$$

where  $\mathcal{V}_k \subset \mathcal{V}$ ,  $\mathcal{E}_k = \{(v_i, v_j) \in \mathcal{E} \mid v_i, v_j \in \mathcal{V}_k\}$ , and  $\mathcal{X}_k, \mathcal{Y}_k$  are the corresponding text attributes and labels. The extraction function  $\Phi$  employs specialized sampling strategies to ensure  $\mathcal{K}$  captures both structural and semantic characteristics of  $\mathcal{G}$  while remaining within LLM context limits.

**Graph Synthesis Process.** The graph synthesis process is formalized as a function  $\Psi : \mathcal{K} \rightarrow \mathcal{G}_s$  that generates new graph elements based on the extracted knowledge:

$$\mathcal{G}_s = \Psi(\mathcal{K}) = (\mathcal{V}_s, \mathcal{E}_s, \mathcal{X}_s, \mathcal{Y}_s), \quad (2)$$

where  $\mathcal{G}_s$  represents the synthesized graph components. Function  $\Psi$  is implemented through our framework that encompasses both semantic understanding and structural pattern recognition.

**Graph Synthesis.** The final enhanced graph merges the original and synthesized components:

$$\mathcal{G}_{\text{new}} = \mathcal{G} \oplus \mathcal{G}_s = (\mathcal{V} \cup \mathcal{V}_s, \mathcal{E} \cup \mathcal{E}_s \cup \mathcal{E}_c, \mathcal{X} \cup \mathcal{X}_s, \mathcal{Y} \cup \mathcal{Y}_s), \quad (3)$$

where  $\mathcal{E}_c = \{(v_i, v_j) \mid v_i \in \mathcal{V}, v_j \in \mathcal{V}_s\}$  represents newly created edges connecting original and synthetic nodes. The quality of  $\mathcal{G}_{\text{new}}$  is evaluated based on both semantic coherence (how well  $\mathcal{X}_s$  aligns with original textual patterns) and structural fidelity (how well  $\mathcal{E}_s$  and  $\mathcal{E}_c$  preserve the topological characteristics of  $\mathcal{G}$ ).

## 3 The Proposed Method

We present GraphMaster, a multi-agent framework conceptualized through the lens of Retrieval-Augmented Generation (RAG) to address the challenges of graph synthesis in data-constrained environments. As illustrated in Figure 1, GraphMaster implements a hierarchical RAG paradigm wherein four specialized LLM-powered agents operate collaboratively in a recursive optimization loop to generate semantically rich and structurally coherent graph extensions.

### 3.1 Framework Overview: RAG-Based Multi-Agent Architecture

GraphMaster formalizes graph synthesis as an iterative RAG process, operating through specialized agents in a closed-loop optimization system. While a single LLM might possess the theoretical capability to understand graph structures, the inherent complexity of generating coherent graph data necessitates a specialized multi-agent approach for three critical reasons. First, real-world graphs substantially exceed typical LLM context windows, requiring strategic sampling and knowledge extraction. Second, maintaining structural consistency across generated elements demands focused attention on connectivity patterns that single-pass generation cannot guarantee. Third, controlling hallucination requires

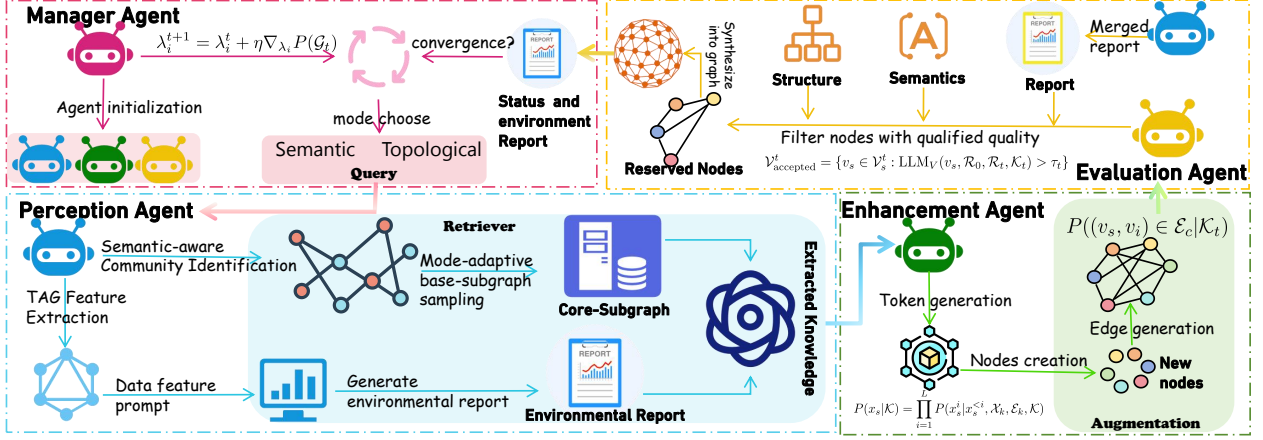


Figure 1: GraphMaster: A hierarchical multi-agent framework for text-attributed graph synthesis.

continuous evaluation and refinement through iterative feedback. A collaborative multi-agent architecture effectively addresses these challenges through specialization and integration:

$$\mathcal{G}_{\text{new}} = \Psi_{\text{RAG}}(\mathcal{G}, \mathcal{Q}, \mathcal{R}, \mathcal{A}_{\text{retrieve}}, \mathcal{A}_{\text{generate}}, \mathcal{A}_{\text{evaluate}}) \quad (4)$$

where  $\mathcal{G}$  is the original graph,  $\mathcal{Q}$  represents the query formulation (enhancement mode),  $\mathcal{R}$  denotes the retrieval strategy, and  $\mathcal{A}_{\text{retrieve}}$ ,  $\mathcal{A}_{\text{generate}}$ , and  $\mathcal{A}_{\text{evaluate}}$  correspond to the agent-specific functions for retrieval, generation, and evaluation, respectively. In each iteration, the Manager Agent formulates the query to guide the synthesis process, the Perception Agent retrieves relevant context to overcome context window limitations, the Enhancement Agent generates new content while maintaining structural consistency, and the Evaluation Agent assesses quality and addresses potential hallucinations—with this cycle continuing until convergence. This collaborative framework enables each agent to focus on a specific challenge while collectively producing coherent graph extensions that a single-pass approach cannot achieve.

### 3.2 Manager Agent: Query Optimization and Control Mechanism

The Manager Agent serves as the meta-cognitive controller that formulates the synthesis query  $\mathcal{Q}_t$  at iteration  $t$  based on a comprehensive environmental status report  $\mathcal{R}_t = \text{LLM}_P(\mathcal{G}_t)$  generated by the Perception Agent. The mode selection function is formalized as:  $M_t = \text{LLM}_M(\mathcal{R}_t) \in \{\text{semantic}, \text{topological}\}$  where  $\text{LLM}_M$  represents the Manager Agent’s reasoning process that analyzes community structures and label distributions captured in  $\mathcal{R}_t$ . This query formulation implements an adaptive mechanism where the Manager optimizes a multi-objective utility function:

$$\omega_t^* = \arg \max_{\omega \in \Omega} [\lambda_1 U_{\text{sem}}(\omega, \mathcal{G}_t) + \lambda_2 U_{\text{struct}}(\omega, \mathcal{G}_t) + \lambda_3 U_{\text{bal}}(\omega, \mathcal{G}_t)] \quad (5)$$

where  $\Omega$  is the strategy space,  $U_{\text{sem}}$ ,  $U_{\text{struct}}$ , and  $U_{\text{bal}}$  represent semantic coherence, structural integrity, and class balance utilities respectively, with adaptive weights  $\lambda_i$  that evolve according to:  $\lambda_i^{t+1} = \lambda_i^t + \eta \nabla_{\lambda_i} P(\mathcal{G}_t)$  where  $P(\mathcal{G}_t)$  measures synthesis progress and  $\eta$  is a learning rate. The Manager orchestrates state transitions, modeled as  $s_{t+1} = T(s_t, a_t, M_t)$ , where states  $s_t$  reflect graph composition and actions  $a_t \in \{a_P, a_E, a_V\}$  correspond to agent invocations for Perception, Enhancement, and Evaluation respectively.

### 3.3 Perception Agent: Context-Aware Corpus Retrieval

The Perception Agent implements the retrieval component of the RAG paradigm, extracting a relevant subgraph from the input graph  $\mathcal{G}_t$  based on the query  $\mathcal{Q}_t = M_t$ . This retrieval process is formalized as:  $\mathcal{K}_t = \mathcal{R}(\mathcal{G}_t, \mathcal{Q}_t) = (\mathcal{V}_k, \mathcal{E}_k, \mathcal{X}_k, \mathcal{Y}_k)$  where  $\mathcal{K}_t$  represents the retrieved knowledge capsule. The retrieval function  $\mathcal{R}$  operates through three sequential stages:

**Semantic-aware Community Identification:** The agent employs a semantic-enriched modularity maximization algorithm to calculate the community distribution of semantic associations for TAG:

$$Q_{\text{sem}} = \frac{1}{2m} \sum_{i,j} \left[ \mathcal{A}_{ij} - \gamma \frac{k_i k_j}{2m} - (1 - \gamma) \frac{d_{\text{sem}}(x_i, x_j)}{\sum_{l,m} d_{\text{sem}}(x_l, x_m)} \right] \delta(c_i, c_j) \quad (6)$$

where  $d_{\text{sem}}(x_i, x_j) = \frac{\mathbf{x}_i \cdot \mathbf{x}_j}{\|\mathbf{x}_i\| \|\mathbf{x}_j\|}$  computes semantic similarity between node attributes,  $k_i$  and  $k_j$  represent the degrees of nodes  $i$  and  $j$ , and  $\gamma$  balances topological and semantic factors.

**Mode-Adaptive Seed Selection Strategy:** Based on the enhancement mode  $M_t$ , the agent selects an optimal seed community  $\mathcal{C}_b$ :

$$\mathcal{C}_b = \begin{cases} \arg \min_i |\mathcal{C}_i| \cdot (1 + \mu \cdot \text{Var}(\{x_j : v_j \in \mathcal{C}_i\})), & \text{if } M_t = \text{semantic}, \\ \{v_j \in \mathcal{V}_{\text{train}} : y_j = \arg \max_c \phi_{\text{imbal}}(c)\}, & \text{if } M_t = \text{topological} \end{cases} \quad (7)$$

where  $\phi_{\text{imbal}}(c) = \max_{c'} |\mathcal{V}_{c'}| / |\mathcal{V}_c|$  quantifies class imbalance,  $\text{Var}$  denotes the variance of node textual features within a community and  $\mu$  weights semantic variance importance. For semantic synthesis, the smaller communities with low internal semantic variance are prefer to be selected to establish a cohesive foundation. For topological synthesis, nodes from minority classes are prioritized.

**Hierarchical Stochastic Diffusion Sampling:** The agent employs a mode-conditional Personalized PageRank (PPR) algorithm, defined as  $\pi^{(k+1)} = \alpha \mathbf{v} + (1 - \alpha) W^T \pi^{(k)}$ , where the teleportation vector  $\mathbf{v}$  varies by enhancement mode:  $v_i = \frac{1}{|\mathcal{C}_b|}$  if  $v_i \in \mathcal{C}_b$  and  $M_t = \text{semantic}$ , or  $v_i = \frac{\mathbb{1}[y_i = \hat{y}]}{\sum_j \mathbb{1}[y_j = \hat{y}]}$  if  $v_i \in \mathcal{V}_{\text{train}}$  and  $M_t = \text{topological}$ , where  $\hat{y} = \arg \min_c |\{v_j \in \mathcal{V}_{\text{train}} : y_j = c\}|$  identifies the label with minimal representation. Following diffusion convergence, the final knowledge subgraph is selected as:

$$\mathcal{K}_t = \{v_i \in \mathcal{S}_{\text{top-}K\%} : r_i < \min(1, \beta \cdot \pi_i / \max_j \pi_j)\} \cap \mathcal{S}_{\text{diverse}} \quad (8)$$

where  $|\mathcal{K}_t| = N$  is constrained by the LLM context window,  $\mathcal{S}_{\text{top-}K\%}$  contains the top  $K\%$  nodes by PPR score,  $r_i \sim \text{Uniform}(0, 1)$  introduces controlled stochasticity, and  $\mathcal{S}_{\text{diverse}}$  ensures community coverage. The environmental status report  $\mathcal{R}_t$  encapsulates multi-scale graph properties:

$$\mathcal{R}_t = \left( \rho_{\text{global}}, \{\rho_{\text{class}}^c\}_{c=1}^C, \{\rho_{\text{comm}}^i\}_{i=1}^{|\mathcal{C}|}, \mathcal{D}_{\text{struct}}, \mathcal{D}_{\text{sem}} \right) \quad (9)$$

where  $\rho_{\text{global}}$  captures global statistics,  $\rho_{\text{class}}^c$  and  $\rho_{\text{comm}}^i$  encode class-level and community-level properties, while  $\mathcal{D}_{\text{struct}}$  and  $\mathcal{D}_{\text{sem}}$  represent structural and semantic distributions.

### 3.4 Enhancement Agent: Context-Conditioned Generation

The Enhancement Agent implements the generation component of the RAG paradigm, synthesizing new graph elements (no more than  $M\%$  of the knowledge subgraph) based on the retrieved knowledge and environmental report. The synthesis process follows Eq. (2) where  $\mathcal{K} = (\mathcal{K}_t, \mathcal{R}_t, M_t)$ . For semantic mode, the LLM generates node attributes using a conditional autoregressive model:

$$P(x_s | \mathcal{K}) = \prod_{i=1}^L P(x_s^i | x_s^{<i}, \mathcal{X}_k, \mathcal{E}_k, \mathcal{K}) \quad (10)$$

where  $x_s^i$  is the  $i$ -th token of attribute  $x_s$ , and  $L$  is the sequence length. This formulation enables the LLM to generate coherent textual attributes that maintain consistency with the knowledge subgraph while introducing appropriate variations.

Crucially, regardless of the current enhancement mode, the agent always generates both node attributes and their connections. For topological mode, the LLM models edge connections between new node  $v_s$  and existing nodes by estimating the probability:

$$P((v_s, v_i) \in \mathcal{E}_c | \mathcal{K}) = \sigma \left( \theta_1 \cdot \text{sim}(x_s, x_i) + \theta_2 \cdot \frac{|\mathcal{N}(v_i) \cap \mathcal{N}_K(v_s)|}{|\mathcal{N}_K(v_s)|} + \theta_3 \cdot \frac{k_i}{\max_j k_j} \right) \quad (11)$$

where  $\mathcal{N}(v_i)$  is the neighborhood of  $v_i$ ,  $\mathcal{N}_K(v_s)$  represents neighbors of  $v_s$  in the knowledge subgraph, and  $\sigma$  is the sigmoid function. The coefficients  $\{\theta_j\}_{j=1}^3$  are dynamically adjusted based on the query mode  $M_t$ . This dual-mode generation enables GraphMaster to adaptively emphasize either semantic coherence or structural fidelity while maintaining integrity across both dimensions.

### 3.5 Evaluation Agent: Multi-dimensional Quality Assessment

The Evaluation Agent implements a comprehensive verification mechanism that integrates four critical information sources:

$$\mathcal{Q}_t = \text{LLM}_V(\mathcal{R}_0, \mathcal{R}_t, \mathcal{K}_t, \mathcal{G}_s^t) \quad (12)$$

where  $\mathcal{Q}_t$  represents the quality assessment outcome,  $\mathcal{R}_0$  is the initial environmental report serving as a baseline,  $\mathcal{R}_t$  is the current environmental report,  $\mathcal{K}_t$  is the retrieved knowledge, and  $\mathcal{G}_s^t$  is the newly synthesized data. The Evaluation Agent simultaneously assesses two key dimensions: **(i) Semantic Coherence:** Evaluates whether the generated textual attributes are contextually appropriate, domain-consistent, and meaningful within the graph’s thematic scope. **(ii) Structural Integrity:** Assesses whether the new edges form logical connections that preserve the original graph’s topological patterns while addressing structural gaps.

For each generated node  $v_s \in \mathcal{V}_s^t$ , the LLM computes a composite quality score, with the final accepted node set defined as:

$$\mathcal{V}_{\text{accepted}}^t = \{v_s \in \mathcal{V}_s^t : \text{LLM}_V(v_s, \mathcal{R}_0, \mathcal{R}_t, \mathcal{K}_t) > \tau_t\} \quad (13)$$

where the threshold  $\tau_t$  is adaptively updated:  $\tau_t = \tau_{t-1} + \zeta(\bar{\mathcal{F}}_t(\omega_t^*) - \bar{\mathcal{F}}_{t-1}(\omega_{t-1}^*))$  with  $\bar{\mathcal{F}}_t(\omega_t^*)$  representing the average quality score at iteration  $t$ . The convergence determination employs a temporal quality gradient analysis:

$$\text{Converged}_t = \mathbb{I} \left( \max_{j \in \{1, \dots, k\}} |\bar{\mathcal{F}}_t(\omega_t^*) - \bar{\mathcal{F}}_{t-j}(\omega_{t-j}^*)| < \epsilon \wedge \text{LLM}_{\text{goal}}(\mathcal{R}_0, \mathcal{R}_t) = \text{True} \right) \quad (14)$$

where  $\mathbb{I}(\cdot)$  is the indicator function and  $\text{LLM}_{\text{goal}}$  assesses whether synthesis objectives have been achieved. If convergence is detected, the Evaluation Agent signals task completion to the Manager Agent; otherwise, it triggers another iteration of the synthesis process<sup>2</sup>.

### 3.6 Time Complexity Analysis

The time complexity of GraphMaster is dominated by three operations: (1) community detection and PPR computation in the Perception Agent, which run in near-linear time  $O(|V_t| + |E_t|)$  on the current graph; (2) LLM inference for node attribute generation and edge probability estimation, which scales with the size  $N$  of the retrieved subgraph rather than the full graph; and (3) quality assessment, which evaluates a fixed number of newly generated nodes against predetermined criteria. Since  $N$  is constrained by the LLM context window and typically small relative to  $|V_t|$ , the LLM operations remain efficient regardless of overall graph size. If the iterative process runs for  $T$  iterations before convergence (generally small due to the Evaluation Agent’s stringent criteria), the overall complexity is  $T$  times the per-iteration cost. This architecture enables GraphMaster to scale effectively by leveraging LLMs for semantic generation on bounded contexts while using efficient graph algorithms for structural computations.

## 4 Experiment

To evaluate GraphMaster comprehensively, we formulate four research questions: **(RQ1):** Can GraphMaster generate high-quality text-attributed graph data in data-limited environment? **(RQ2):** Can the graph data synthesized by GraphMaster retain the original graph features well? **(RQ3):** What is the relative contribution of each component in GraphMaster to the overall synthesis quality? **(RQ4):** Can GraphMaster maintain interpretability well?

<sup>2</sup>Note that a recent model called GAG [17] also focuses on using agents to achieve data synthesis. We introduce the differences between GraphMaster and GAG in detail in Appendix B.

## 4.1 Overall Performance (RQ1)

We evaluate GraphMaster’s ability to synthesize high-quality graph data by applying it to enhance the data-limited datasets we created and assessing whether the enhanced datasets improve downstream model performance. We employ standard metrics including Accuracy and F1 Score as evaluation criteria, with higher values indicating superior performance.

**Baselines and Datasets.** The comparative baselines are categorized into five groups: (1) original TAG training without data synthesis; (2) Classic data augmentation methods: GAUGO [41]; (3) LLM-based data augmentation methods: GraphEdit [12] and LLM4RGNN [39]; (4) Classic data synthesis methods: GraphSmote [40], G-Mixup [14], IntraMix [42], GraphAdasyn [21], FG-SMOTE [34], and AGMixup [22]; (5) LLM-based data synthesis methods: GAG [17] and note that there are very limited baselines for TAG synthesis using LLM, and we created these two additional baselines named Mixed-LLM and Synthesis-LLM, whose implementations can be found in the Appendix C. Our experiments utilize six widely recognized text-attributed graph datasets: Cora [24], Citeseer [11], Wikics [8], Arxiv2023 [28], and History and Children [37]. It is worth noting that in order to better simulate the data-limited environment to test the effect of data synthesis, we created 6 data-limited datasets, namely SubCora, SubCiteseer, SubWikics, SubHistory, SubArxiv2023, and SubChildren (details are given in Appendix D). In this article, unless otherwise specified, we assume that the augmentation-based method uses the original dataset, while the synthesis-based method uses the data-limited dataset we created. For downstream task evaluation, we implement four established graph neural network architectures: GCN [18], JKNET [35], GraphSage [13] and GAT [30].

**Implement Details.** We ran the entire experiment on an 80G A100 GPU, using the QwQ-32B model [29] as the base LLM and enabling it to assume different agent roles through iterative calls. For the background knowledge nodes, we set  $N = 30$ , and for the newly generated nodes, we configured  $M\% = 15\%$  (The hyperparameter sensitivity analysis are given in Appendix F). In training the GNN model, we first initialized the text attributes with Sentence-BERT [27] to generate the initial features before proceeding with training. To ensure the robustness of our experiments, we repeated each experiment 50 times and reported the mean and standard deviation of the results.

Table 1: Comparison of GraphMaster with other TAG synthesis methods in GCN model. Best performance is indicated by the **bold** face numbers, and the underline means the second best. ‘Acc’ and ‘F1’ are short for Accuracy and F1 Score, respectively.

Type	Model	Cora		Citeseer		Wikics		History		Arxiv2023		Children	
		Acc	F1	Acc	F1	Acc	F1	Acc	F1	Acc	F1	Acc	F1
Original	Original Model	88.9±1.1	88.5±1.5	78.1±1.1	75.0±0.3	79.7±0.8	77.8±0.3	84.2±0.6	43.1±0.3	76.3±1.0	54.9±0.5	52.6±0.7	32.3±1.5
Classic-Aug	GAUGO	88.9±0.8	88.0±1.0	78.1±0.7	77.2±0.3	79.9±0.9	77.7±0.7	84.6±1.5	44.7±0.6	76.8±1.4	53.0±0.3	51.8±0.6	33.6±0.7
LLM-Aug	GraphEdit	91.0±0.9	89.7±0.6	81.9±0.9	80.8±1.1	82.0±1.1	80.7±1.2	87.6±0.6	45.7±1.3	78.0±0.9	57.8±0.3	54.3±0.7	35.7±1.4
	LLM4RGNN	91.2±0.6	88.8±1.1	80.9±1.3	76.6±1.1	83.6±1.4	81.6±1.5	88.9±0.7	48.6±0.4	79.3±1.1	59.1±0.4	55.7±1.4	36.7±0.8
Classic-Syn	GraphSmote	88.7±1.4	87.4±1.1	78.1±0.5	74.6±1.4	80.7±1.5	78.6±1.4	84.9±0.5	43.9±0.3	76.2±0.4	55.5±0.4	53.1±0.9	33.2±0.6
	G-Mixup	87.4±1.1	87.0±0.7	78.2±0.9	76.8±1.1	79.7±0.4	78.0±0.8	84.6±0.6	43.6±0.6	76.6±0.4	56.5±0.3	53.0±0.6	33.0±0.3
	IntraMix	80.9±0.6	82.8±0.7	71.3±0.8	70.7±0.5	73.7±1.0	74.5±0.4	82.4±1.5	42.7±0.6	72.4±1.1	53.9±0.8	45.2±0.9	30.1±0.7
	GraphAdasyn	89.2±0.3	88.7±0.5	78.9±1.0	78.4±1.4	80.8±1.2	78.9±0.7	84.6±1.5	46.1±0.8	77.5±0.7	57.0±1.1	53.6±0.5	33.0±0.6
	FG-SMOTE	88.9±1.5	87.6±1.0	78.7±0.8	74.7±1.4	81.0±0.8	79.0±1.0	85.0±1.4	44.0±0.9	76.4±1.2	55.8±1.4	53.1±1.5	33.3±0.9
	AGMixup	84.7±0.4	86.6±0.4	71.7±0.9	73.2±1.1	78.8±0.9	76.6±1.1	81.8±0.9	42.9±0.3	76.8±1.1	53.7±0.5	53.6±1.0	32.6±0.8
LLM-Syn	GAG	91.0±1.2	89.3±0.4	82.8±0.9	80.0±1.5	84.9±1.3	83.2±0.7	88.9±0.5	49.8±0.8	79.9±0.5	59.4±1.0	56.7±0.8	38.0±0.5
	Mixed-LLM	89.9±0.5	89.3±0.4	83.5±0.9	81.3±0.8	84.9±0.9	83.4±0.8	89.2±1.3	55.8±0.8	81.4±1.5	61.2±0.9	60.0±0.7	39.6±0.7
	Synthesis-LLM	89.8±1.3	89.1±1.0	84.5±1.0	82.7±1.1	84.8±0.4	83.2±0.5	89.4±1.3	53.4±1.3	81.0±1.2	62.3±0.8	60.9±1.0	40.1±0.9
	<b>GraphMaster</b>	<b>92.6±1.0</b>	<b>91.3±1.0</b>	<b>87.5±0.9</b>	<b>86.4±1.1</b>	<b>86.6±0.8</b>	<b>85.4±0.9</b>	<b>91.3±1.3</b>	<b>62.1±1.4</b>	<b>86.7±1.3</b>	<b>65.5±1.5</b>	<b>67.7±1.4</b>	<b>46.7±1.3</b>

**Results.** As shown in Table 1 (Due to space limitation, other three models’ results are given in Appendix G.), GraphMaster consistently outperforms all baselines, demonstrating the superiority of our approach. Notably, we observed that some baseline methods even yield lower performance than the original dataset. This is primarily because traditional graph synthesis techniques fail to capture the semantic nuances of sentences; consequently, when using Sentence-BERT embeddings instead of bag-of-words representations, their effectiveness is significantly diminished. Moreover, the other LLM-based baselines we compared against mainly focus on anti-interference detection or data synthesis on other scenarios rather than TAG data synthesis, resulting in their performance being significantly lower than that of GraphMaster, which targets TAG data synthesis. Finally, the two LLM-based TAG synthesis baselines we developed show significant advantages over traditional baselines. However, since they cannot fully understand the semantics and topological structure of TAG, although they are higher than other baselines, they are still significantly lower than GraphMaster.

## 4.2 Synthetic Graph Feature Analysis (RQ2)

Our second research question examines whether the new graph data generated by GraphMaster in data-limited environments can maintain consistency with the original graph’s structural features. We conducted a comprehensive

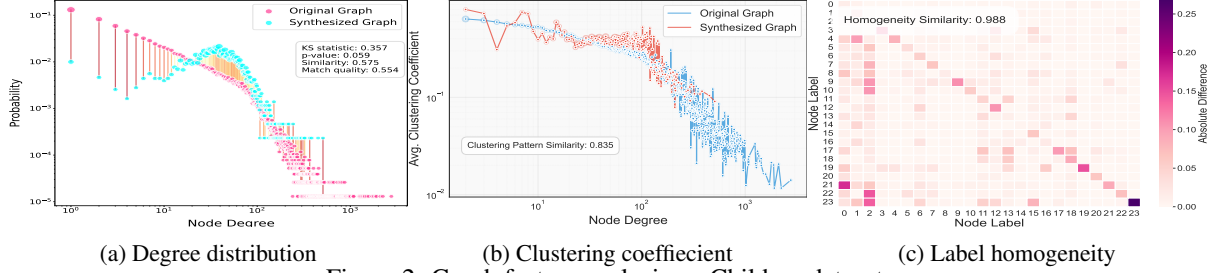


Figure 2: Graph feature analysis on Children dataset.

analysis across three dimensions: degree distribution, clustering coefficient, and label homogeneity. As shown in Figure 2, GraphMaster demonstrates excellent performance in preserving the network’s topological backbone. For example, the two-sample Kolmogorov–Smirnov test statistic between the degree distributions of the original and synthesized Children graphs is 0.357 ( $p = 0.059$ ), indicating no statistically significant difference. The clustering coefficient similarity score is 0.835, which represents a substantial improvement over the original data-limited Children graph (0.785). Concurrently, the label homogeneity similarity reaches an impressive 0.988 (the heatmap of label–label connection frequencies is almost identical for original vs. synthetic), indicating minimal differences in class mixing patterns. These characteristics show that GraphMaster can generate high-quality synthetic graphs that retain key structural properties of the original data. (Additional graph comparison figures are provided in Appendix H.)

### 4.3 Ablation Study (RQ3)

Table 2: Ablation experiment in GCN model.

model	Cora		Citeseer		Wikies		History		Arxiv2023		Children	
	Acc	F1	Acc	F1	Acc	F1	Acc	F1	Acc	F1	Acc	F1
QwQ-32B	<b>92.6</b> ± 1.0	<b>91.3</b> ± 1.0	<b>87.5</b> ± 0.9	<b>86.4</b> ± 1.1	<b>86.6</b> ± 0.8	<b>85.4</b> ± 0.8	<b>91.3</b> ± 1.3	<b>62.1</b> ± 1.4	<b>86.7</b> ± 1.3	<b>65.5</b> ± 1.5	<b>67.7</b> ± 1.4	<b>46.7</b> ± 1.3
Qwen-32B	92.0 ± 0.9	91.1 ± 0.9	86.9 ± 1.1	85.8 ± 1.0	86.1 ± 0.9	84.7 ± 0.9	90.9 ± 1.2	61.6 ± 0.9	86.1 ± 0.8	64.9 ± 1.1	67.1 ± 1.1	46.4 ± 1.0
DeepSeek-R1-32B	92.3 ± 0.8	92.1 ± 0.8	87.3 ± 1.0	86.3 ± 1.1	86.2 ± 0.8	85.1 ± 0.9	91.0 ± 1.2	61.8 ± 0.9	86.3 ± 1.0	65.2 ± 1.2	67.5 ± 1.2	46.6 ± 1.4
LLaMA-33B	91.9 ± 0.9	90.9 ± 1.1	86.3 ± 0.8	85.4 ± 1.2	85.9 ± 0.5	84.5 ± 0.6	90.8 ± 0.7	61.4 ± 0.9	85.7 ± 0.7	64.7 ± 0.8	67.0 ± 0.9	46.2 ± 0.9
w.o Perception Agent	90.2 ± 0.8	89.9 ± 0.3	84.7 ± 0.7	83.3 ± 1.1	85.1 ± 0.7	84.2 ± 0.3	89.8 ± 1.1	58.8 ± 0.9	82.3 ± 0.5	63.4 ± 0.9	63.6 ± 1.3	44.8 ± 0.7
w.o Evaluation Agent	91.3 ± 0.7	90.4 ± 0.7	85.6 ± 0.4	85.1 ± 0.9	85.8 ± 0.9	84.4 ± 0.6	90.3 ± 0.7	60.7 ± 0.7	84.7 ± 0.9	63.9 ± 1.1	64.7 ± 1.1	45.5 ± 1.3
N=20	92.1 ± 0.8	90.8 ± 0.5	87.0 ± 0.7	85.9 ± 0.8	86.0 ± 0.6	84.6 ± 0.7	90.6 ± 0.8	61.5 ± 0.8	86.0 ± 0.7	64.8 ± 0.7	67.2 ± 0.8	46.3 ± 0.6
N=30	<b>92.6</b> ± 1.0	<b>91.3</b> ± 1.0	<b>87.5</b> ± 0.9	<b>86.4</b> ± 1.1	<b>86.6</b> ± 0.8	<b>85.4</b> ± 0.8	<b>91.3</b> ± 1.3	<b>62.1</b> ± 1.4	<b>86.7</b> ± 1.3	<b>65.5</b> ± 1.5	<b>67.7</b> ± 1.4	<b>46.7</b> ± 1.3
N=40	92.4 ± 0.9	91.1 ± 0.9	87.2 ± 0.8	86.1 ± 1.0	86.4 ± 0.7	85.2 ± 0.7	91.1 ± 1.2	61.9 ± 1.3	86.5 ± 1.2	65.3 ± 1.4	67.5 ± 1.3	46.5 ± 1.2
M=10%	92.3 ± 0.9	91.0 ± 0.9	87.1 ± 0.7	86.0 ± 0.9	86.3 ± 0.6	85.0 ± 0.7	91.0 ± 1.1	61.7 ± 1.2	86.4 ± 1.1	65.1 ± 1.3	67.4 ± 1.2	46.4 ± 1.1
M=15%	<b>92.6</b> ± 1.0	<b>91.3</b> ± 1.0	<b>87.5</b> ± 0.9	<b>86.4</b> ± 1.1	<b>86.6</b> ± 0.8	<b>85.4</b> ± 0.8	<b>91.3</b> ± 1.3	<b>62.1</b> ± 1.4	<b>86.7</b> ± 1.3	<b>65.5</b> ± 1.5	<b>67.7</b> ± 1.4	<b>46.7</b> ± 1.3
M=20%	92.0 ± 0.8	90.7 ± 0.8	86.8 ± 0.6	85.7 ± 0.8	85.9 ± 0.5	84.5 ± 0.6	90.5 ± 0.7	61.2 ± 0.8	85.9 ± 0.6	64.6 ± 0.6	67.0 ± 0.7	46.1 ± 0.5

In this section, we investigate the relative importance of various components within the GraphMaster framework and their impact on synthesis quality. We systematically analyze how different agent configurations affect the overall performance. Meanwhile, we studied the impact of different LLM models on the number of graph synthesis. We selected Qwen-32B [1], Deepseek-R1-32B [5] and Llama-33B [4], three models with parameters around 32B as control models. Additionally, we examine how varying the size of the background knowledge base ( $N = |K|$ ) and the percentage of newly generated nodes ( $M\%$ ) to background knowledge nodes influences the synthesis effectiveness and quality of the generated graph data.

We trained the model using GCN on six datasets, and the results are presented in Table 2. Our findings indicate that the performance of the synthesized graph data varies across different large language models. For instance, despite LLaMA-33B having the largest number of parameters, its synthesized graph data quality is inferior to that produced by QwQ-32B. Additionally, the absence of any one agent significantly degrades the overall model performance, underscoring the necessity of our multi-agent framework. Finally, with regard to both the size of the background knowledge base and the percentage of new nodes generated per round, we observed that performance initially improves with an increase in these values; however, beyond a certain threshold, further increases lead to performance degradation. This demonstrates that an excessive amount of background knowledge may obscure the model’s focus, and generating too high a proportion of new nodes may not yield additional benefits, given the inherent limitations in the model’s capacity for innovation.

### 4.4 Interpretability Analysis (RQ4)

To evaluate the transparency of our GraphMaster model, we conduct both human-centered and algorithmic assessments of interpretability (theoretical details in Appendix I). For human evaluation, 50 expert reviewers rated 200 synthesis



instances across three dimensions: process transparency, decision justification, and outcome predictability. The overall Traceability Score quantifies how well humans understand the generation process:

$$T_{\text{score}} = \frac{1}{R \cdot N} \sum_{r=1}^R \sum_{i=1}^N t_{r,i}, \quad (15)$$

where  $t_{r,i}$  represents the score given by reviewer  $r$  for instance  $i$ . In parallel, we leverage a Grassmann manifold-based approach to systematically assess semantic consistency of synthesized nodes. This mathematical framework provides a principled way to measure how well generated nodes align with the semantic direction of background knowledge, yielding coherence scores in the range  $[0, 1]$ .

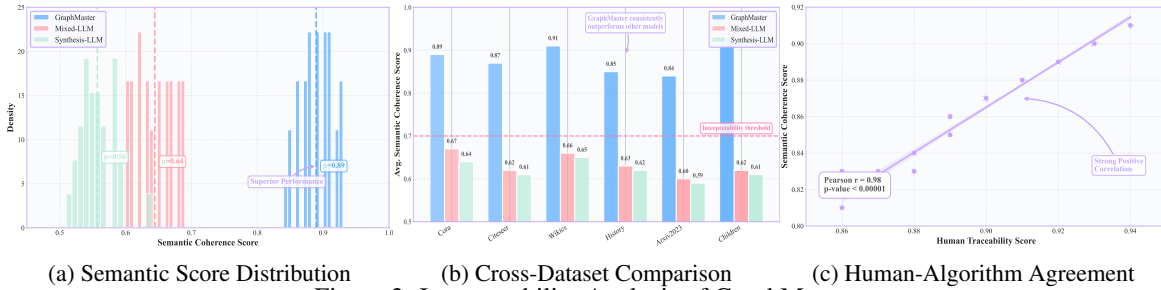


Figure 3: Interpretability Analysis of GraphMaster.

Our human evaluation results demonstrate that GraphMaster exhibits excellent interpretability, with an average traceability score of  $T_{\text{score}} = 0.92$ , significantly outperforming Mixed-LLM (0.66) and Synthesis-LLM (0.59). For the Grassmann manifold-based evaluation method, Figure 3a shows that GraphMaster significantly outperforms comparative methods in terms of semantic coherence, indicating that GraphMaster can generate nodes highly aligned with the principal semantic direction. The score distribution more concentrated in higher value regions also indicates stronger consistency in the quality of generated nodes. Figure 3b shows that GraphMaster maintains high performance across all datasets, consistently exceeding the interpretability threshold of 0.7. Figure 3c demonstrates a strong correlation between human ratings and semantic coherence scores ( $r=0.78$ ,  $p<0.00001$ ), further validating our Grassmann manifold-based approach as an effective metric for measuring interpretability. This alignment between human judgment and geometric measures confirms the practical relevance and feasibility of our mathematical framework.

## 5 Conclusion

In this paper, we introduced GraphMaster, the first multi-agent framework for text-attributed graph synthesis that successfully addresses the critical bottleneck of data scarcity in training GFM. By orchestrating specialized LLM agents in a hierarchical RAG paradigm, our approach systematically overcomes the limitations of traditional synthesis methods, generating semantically rich and structurally coherent graph extensions even in severely data-constrained environments. Beyond the framework itself, we created specialized data-limited variants of six standard graph benchmarks to provide a standardized testbed for future research in data-scarce graph learning. Furthermore, we developed a novel dual-perspective interpretability assessment methodology that combines expert human evaluation with a theoretically grounded Grassmannian manifold-based analysis, offering unprecedented insights into the semantic quality of synthesized graph data. Comprehensive experiments demonstrate GraphMaster’s consistently superior performance across diverse datasets and downstream GNN architectures, while maintaining high transparency throughout the synthesis process. This work not only provides an immediate solution to the graph data scarcity problem but also establishes foundational datasets and evaluation methodologies for advancing the field of interpretable graph data synthesis.

## References

- [1] Jinze Bai, Shuai Bai, Yunfei Chu, Zeyu Cui, Kai Dang, Xiaodong Deng, Yang Fan, Wenbin Ge, Yu Han, Fei Huang, Binyuan Hui, Luo Ji, Mei Li, Junyang Lin, Runji Lin, Dayiheng Liu, Gao Liu, Chengqiang Lu, Keming Lu, Jianxin Ma, Rui Men, Xingzhang Ren, Xuancheng Ren, Chuanqi Tan, Sinan Tan, Jianhong Tu, Peng Wang, Shijie Wang, Wei Wang, Shengguang Wu, Benfeng Xu, Jin Xu, An Yang, Hao Yang, Jian Yang, Shusheng Yang, Yang Yao, Bowen Yu, Hongyi Yuan, Zheng Yuan, Jianwei Zhang, Xingxuan Zhang, Yichang Zhang, Zhenru Zhang, Chang Zhou, Jingren Zhou, Xiaohuan Zhou, and Tianhang Zhu. Qwen technical report. *arXiv preprint arXiv:2309.16609*, 2023.
- [2] Tom B. Brown, Benjamin Mann, Nick Ryder, Melanie Subbiah, Jared Kaplan, Prafulla Dhariwal, Arvind Neelakantan, Pranav Shyam, Girish Sastry, Amanda Askell, et al. Language models are few-shot learners. *Advances in Neural Information Processing Systems*, 33:1877–1901, 2020.
- [3] Yung-Sung Chuang, Linlu Qiu, Cheng-Yu Hsieh, Ranjay Krishna, Yoon Kim, and James Glass. Lookback lens: Detecting and mitigating contextual hallucinations in large language models using only attention maps. *arXiv preprint arXiv:2407.07071*, 2024.
- [4] Cognitive Computations. Samantha: A sentient ai assistant trained in philosophy, psychology, and personal relationships, 2024. <https://huggingface.co/cognitivecomputations/samantha-1.1-llama-33b>.
- [5] DeepSeek-AI. Deepseek-r1: Incentivizing reasoning capability in llms via reinforcement learning, 2025.
- [6] Kaize Ding, Zhe Xu, Hanghang Tong, and Huan Liu. Data augmentation for deep graph learning: A survey. *SIGKDD Explorations*, 24(2):61–79, 2023.
- [7] Alexey Dosovitskiy, Lucas Beyer, Alexander Kolesnikov, Dirk Weissenborn, Xiaohua Zhai, Thomas Unterthiner, Mostafa Dehghani, Matthias Minderer, Georg Heigold, Sylvain Gelly, et al. An image is worth 16x16 words: Transformers for image recognition at scale. In *International Conference on Learning Representations*, 2020.
- [8] Vijay Prakash Dwivedi, Chaitanya K Joshi, Anh Tuan Luu, Thomas Laurent, Yoshua Bengio, and Xavier Bresson. Benchmarking graph neural networks. *arXiv preprint arXiv:2003.00982*, 2020.
- [9] Yushi Feng, Tsai Hor Chan, Guosheng Yin, and Lequan Yu. Democratizing large language model-based graph data augmentation via latent knowledge graphs. *arXiv preprint arXiv:2502.13535*, 2025.
- [10] Jingtong Gao, Xiangyu Zhao, Bo Chen, Fan Yan, Huifeng Guo, and Ruiming Tang. Autotransfer: Instance transfer for cross-domain recommendations. In *Proceedings of the 46th International ACM SIGIR Conference on Research and Development in Information Retrieval (SIGIR '23)*, pages 1478–1487. ACM, 2023.
- [11] C. Lee Giles, Kurt Bollacker, and Steve Lawrence. Citeseer: An automatic citation indexing system. In *Proceedings of the Third ACM Conference on Digital Libraries*, pages 89–98, 1998.
- [12] Zirui Guo, Lianghao Xia, Yanhua Yu, Yuling Wang, Zixuan Yang, Wei Wei, Liang Pang, Tat-Seng Chua, and Chao Huang. Graphedit: Large language models for graph structure learning. In *Proceedings of [Conference Name]*, 2025. Preprint available at <https://github.com/HKUDS/GraphEdit>.
- [13] William L. Hamilton, Zitao Ying, and Jure Leskovec. Inductive representation learning on large graphs. In *Advances in Neural Information Processing Systems (NeurIPS)*, 2017.
- [14] Xiaotian Han, Zhimeng Jiang, Ninghao Liu, and Xia Hu. G-mixup: Graph data augmentation for graph classification. In *Proceedings of the 39th International Conference on Machine Learning (ICML)*, volume 162, pages 8866–8882. PMLR, 2022.
- [15] Ziniu Hu, Yuxiao Dong, Kuansan Wang, Kai-Wei Chang, and Yizhou Sun. Gpt-gnn: Generative pre-training of graph neural networks. In *Proceedings of the 26th ACM SIGKDD International Conference on Knowledge Discovery & Data Mining (KDD '20)*, pages 1857–1867. ACM, 2020.
- [16] Jiarui Ji, Runlin Lei, Jialing Bi, Zhewei Wei, Xu Chen, Yankai Lin, Xuchen Pan, Yaliang Li, and Bolin Ding. LLM-Based Multi-Agent Systems are Scalable Graph Generative Models. *arXiv preprint arXiv:2410.09824*, 2025.
- [17] Jiarui Ji, Runlin Lei, Jialing Bi, Zhewei Wei, Xu Chen, Yankai Lin, Xuchen Pan, Yaliang Li, and Bolin Ding. Llm-based multi-agent systems are scalable graph generative models. *arXiv preprint arXiv:2410.09824*, 2025.
- [18] Thomas N. Kipf and Max Welling. Semi-supervised classification with graph convolutional networks. In *International Conference on Learning Representations (ICLR)*, 2017.
- [19] Dugang Liu, Chaohua Yang, Xing Tang, Yejing Wang, Fuyuan Lyu, Weihong Luo, Xiuqiang He, Zhong Ming, and Xiangyu Zhao. Multifs: Automated multi-scenario feature selection in deep recommender systems. In *Proceedings of the 17th ACM International Conference on Web Search and Data Mining (WSDM '24)*, pages 434–442. ACM, 2024.

- [20] Jiawei Liu, Cheng Yang, Zhiyuan Lu, Junze Chen, Yibo Li, Mengmei Zhang, Ting Bai, Yuan Fang, Lichao Sun, Philip S. Yu, and Chuan Shi. Graph foundation models: Concepts, opportunities and challenges. *IEEE Transactions on Pattern Analysis and Machine Intelligence*, 2024. Preprint version available on arXiv.
- [21] Guangquan Lu, Wanxin Chen, Yadan Han, Jiamin Tang, and Faliang Huang. Joint graph augmentation and adaptive synthetic sampling for imbalanced node classification. In *Proceedings of [Conference Name]*, 2025.
- [22] Weigang Lu, Ziyu Guan, Wei Zhao, Yaming Yang, Yibing Zhan, Yiheng Lu, and Dapeng Tao. Agmixup: Adaptive graph mixup for semi-supervised node classification. In *Proceedings of [Conference Name]*, 2025. Preprint available at <https://github.com/WeigangLu/AGMixup>.
- [23] Haitao Mao, Zhikai Chen, Wenzhuo Tang, Jianan Zhao, Yao Ma, Tong Zhao, Neil Shah, Mikhail Galkin, and Jiliang Tang. Position: Graph foundation models are already here. arXiv preprint arXiv:2402.02216, 2024. Version 3, revised on 30 May 2024.
- [24] Andrew McCallum, Kamal Nigam, et al. Automating the construction of internet portals with machine learning. In *Proceedings of the Seventh International Conference on Machine Learning*, pages 79–86, 2000.
- [25] Nick McKenna, Tianyi Li, Liang Cheng, Mohammad Javad Hosseini, Mark Johnson, and Mark Steedman. Sources of hallucination by large language models on inference tasks. *arXiv preprint arXiv:2305.14552*, 2023.
- [26] Xuchen Pan, Dawei Gao, Yuexiang Xie, Yushuo Chen, Zhewei Wei, Yaliang Li, and Bolin Ding. Very Large-Scale Multi-Agent Simulation in AgentScope. arXiv preprint arXiv:2407.17789, 2024.
- [27] Nils Reimers and Iryna Gurevych. Sentence-bert: Sentence embeddings using siamese BERT-networks. In *Proceedings of the 2019 Conference on Empirical Methods in Natural Language Processing (EMNLP)*, Hong Kong, China, 2019. Association for Computational Linguistics.
- [28] Laurent Rigoux, Xavier Brown, Thomas Laurent, Adam Predel, Yann LeCun, and Bryan Hooi. Harnessing explanations: Llm-to-llm interpreter for enhanced text-attributed graph representation learning. In *Proceedings of the International Conference on Learning Representations (ICLR)*, 2024. arXiv:2013.105235v5 [cs.LG].
- [29] Qwen Team. Qwq-32b: Embracing the power of reinforcement learning, March 2025.
- [30] Petar Velicković, Guillem Cucurull, Arantxa Casanova, Adriana Romero, Pietro Lio, and Yoshua Bengio. Graph attention networks. In *International Conference on Learning Representations (ICLR)*, 2018.
- [31] Vikas Verma, Alex Lamb, Christopher Beckham, Amir Najafi, Ioannis Mitliagkas, David Lopez-Paz, and Yoshua Bengio. Manifold mixup: Better representations by interpolating hidden states. In *Proceedings of the 36th International Conference on Machine Learning (ICML)*, pages 6438–6447. PMLR, 2019.
- [32] Yiwei Wang, Wei Wang, Yuxuan Liang, Yujun Cai, Juncheng Liu, and Bryan Hooi. Nodeaug: Semi-supervised node classification with data augmentation. In *Proceedings of the 26th ACM SIGKDD Conference on Knowledge Discovery and Data Mining (KDD)*, pages 207–217. ACM, 2020.
- [33] Yizhong Wang, Yeganeh Kordi, Swaroop Mishra, Alisa Liu, Noah A. Smith, Daniel Khashabi, and Hannaneh Hajishirzi. SELF-INSTRUCT: Aligning language models with self-generated instructions. arXiv preprint arXiv:2212.10560, 2023.
- [34] Zichong Wang, Zhipeng Yin, Yuying Zhang, Liping Yang, Tingting Zhang, Niki Pissinou, Yu Cai, Shu Hu, Yun Li, Liang Zhao, and Wenbin Zhang. Fg-smote: Towards fair node classification with graph neural network. In *Proceedings of [Conference Name]*, 2025.
- [35] Keyulu Xu, Weihua Hu, Jure Leskovec, and Stefanie Jegelka. Jumping knowledge networks. In *International Conference on Learning Representations (ICLR)*, 2018.
- [36] Yao Xu, Shizhu He, Jiabei Chen, et al. Generate-on-Graph: Treat llm as both agent and kg for incomplete knowledge graph question answering. arXiv preprint arXiv:2404.14741, 2024.
- [37] Hao Yan, Chaozhuo Li, Ruosong Long, Chao Yan, Jianan Zhao, Wenwen Zhuang, Jun Yin, Peiyan Zhang, Weihao Han, Hao Sun, et al. A comprehensive study on text-attributed graphs: Benchmarking and rethinking. *Advances in Neural Information Processing Systems*, 36:17238–17264, 2023.
- [38] Hongyi Zhang, Moustapha Cisse, Yann N Dauphin, and David Lopez-Paz. mixup: Beyond empirical risk minimization. In *International Conference on Learning Representations (ICLR)*, 2018.
- [39] Zhongjian Zhang, Xiao Wang, Huichi Zhou, Yue Yu, Mengmei Zhang, Cheng Yang, and Chuan Shi. Can large language models improve the adversarial robustness of graph neural networks? In *Proceedings of the 31st ACM SIGKDD Conference on Knowledge Discovery and Data Mining (KDD '25)*, pages 1–14, 2025.
- [40] Tianxiang Zhao, Xiang Zhang, and Suhang Wang. Graphsmote: Imbalanced node classification on graphs with graph neural networks. In *Proceedings of the Fourteenth ACM International Conference on Web Search and Data Mining (WSDM)*, pages 833–841. ACM, 2021.

- 
- [41] Tong Zhao, Yozen Liu, Leonardo Neves, Oliver Woodford, Meng Jiang, and Neil Shah. Data augmentation for graph neural networks. In *Proceedings of the AAAI Conference on Artificial Intelligence*, volume 35, pages 11015–11023, 2021.
  - [42] Shenghe Zheng, Hongzhi Wang, and Xianglong Liu. Intramix: Intra-class mixup generation for accurate labels and neighbors, 2024. Accepted by NeurIPS2024.
  - [43] Jiajun Zhou, Jie Shen, and Qi Xuan. Data augmentation for graph classification. In *Proceedings of the 29th ACM International Conference on Information and Knowledge Management (CIKM '20)*, pages 2341–2348. ACM, 2020.

## A Theoretical Analysis of Agent Capabilities

In this appendix, we present rigorous theoretical analyses validating the effectiveness of GraphMaster’s agent components. We first develop a foundational mathematical framework for each agent’s operations, then derive formal guarantees regarding their synthesis capabilities through a series of interconnected theorems and propositions.

### A.1 Information-Theoretic Analysis of the Perception Agent

We establish a theoretical framework for analyzing the information capture capabilities of the Perception Agent through the lens of information theory and spectral graph theory.

**Definition 1** (Topological Information Density). *For a text attribute graph  $\mathcal{G} = (\mathcal{V}, \mathcal{E}, \mathcal{X}, \mathcal{Y})$ , the topological information density  $\mathcal{I}(\mathcal{G})$  is defined as:*

$$\mathcal{I}(\mathcal{G}) = \frac{1}{|\mathcal{V}|} \sum_{v_i \in \mathcal{V}} \left[ H(p_{\mathcal{N}(v_i)}) + \sum_{v_j \in \mathcal{N}(v_i)} KL(p_{v_j} | p_{\mathcal{G}}) \right] \quad (16)$$

where  $H(\cdot)$  is the entropy function,  $p_{\mathcal{N}(v_i)}$  is the probability distribution over the neighborhood of  $v_i$ ,  $p_{v_j}$  is the local distribution at node  $v_j$ , and  $p_{\mathcal{G}}$  is the global distribution over the graph.

**Theorem 1** (Information Capture Properties of the Perception Agent). *Given a text-attributed graph  $\mathcal{G} = (\mathcal{V}, \mathcal{E}, \mathcal{X}, \mathcal{Y})$ , the Perception Agent constructs:*

1. An environment report  $\mathcal{R}_t$  that preserves topological information with bounded distortion:

$$DKL(\mathcal{I}(\mathcal{G}) | \mathcal{I}(\mathcal{R}_t)) \leq \epsilon_t + O\left(\frac{\log |\mathcal{V}|}{|\mathcal{V}|}\right) \quad (17)$$

2. A knowledge encapsulation  $\mathcal{K}_t$  that preserves semantic relationships with high fidelity:

$$\mathbb{P}\left(\sup_{v_i, v_j \in \mathcal{V}} \left| \mathcal{S}(x_i, x_j) - \hat{\mathcal{S}}(x_i, x_j; \mathcal{K}_t) \right| > \delta\right) \leq 2 \exp\left(-\frac{2|\mathcal{K}_t|\delta^2}{C_S^2}\right) \quad (18)$$

where  $\mathcal{S}(\cdot, \cdot)$  is a semantic similarity function,  $\hat{\mathcal{S}}(\cdot, \cdot; \mathcal{K}_t)$  is its empirical estimate based on  $\mathcal{K}_t$ , and  $C_S$  is a problem-specific constant.

*Proof.* We decompose the proof into topological and semantic components.

#### Part 1: Topological Information Preservation

The environment report  $\mathcal{R}_t = (\rho_{\text{global}}, \{\rho_{\text{class}}^c\}_{c=1}^C, \{\rho_{\text{comm}}^i\}_{i=1}^{|\mathcal{C}|}, \mathcal{D}_{\text{struct}}, \mathcal{D}_{\text{sem}})$  encodes a compressed representation of the graph’s topological properties. We establish information-theoretic bounds on this compression.

For the degree distribution captured in  $\mathcal{D}_{\text{struct}}$ :

$$W_2(P_{\text{deg}}^{\mathcal{G}}, P_{\text{deg}}^{\mathcal{R}_t})^2 \leq \frac{C_1 \log |\mathcal{V}|}{|\mathcal{V}|} \quad (19)$$

where  $W_2$  is the 2-Wasserstein distance and  $C_1$  is a universal constant.

For spectral properties, the Laplacian spectrum satisfies:

$$\left| \frac{\lambda_i(\mathcal{G})}{\lambda_{\max}(\mathcal{G})} - \frac{\rho_i}{\rho_{\max}} \right| \leq C_2 \sqrt{\frac{\log |\mathcal{V}|}{|\mathcal{V}|}} \quad (20)$$

where  $\lambda_i(\mathcal{G})$  is the  $i$ -th eigenvalue of the normalized Laplacian of  $\mathcal{G}$ , and  $\rho_i$  is the corresponding encoded value in  $\rho_{\text{global}}$ .

The community structure preservation follows from the Cheeger’s inequality:

$$\mathcal{R}_t \text{ encodes } h_{\mathcal{G}}(S_i) \text{ such that } \frac{\lambda_2(\mathcal{G})}{2} \leq h_{\mathcal{G}}(S_i) \leq \sqrt{2\lambda_2(\mathcal{G})} \quad (21)$$

where  $h_{\mathcal{G}}(S_i)$  is the Cheeger constant for community  $S_i$ .

By aggregating these bounds and applying the data processing inequality, we establish the KL-divergence bound on topological information.

## Part 2: Semantic Preservation

The knowledge encapsulation  $\mathcal{K}t$  is constructed via semantic-enriched modularity maximization and personalized PageRank sampling:

$$Q_{\text{sem}} = \frac{1}{2m} \sum_{i,j} \left[ A_{ij} - \gamma \frac{k_i k_j}{2m} - (1 - \gamma) \frac{d_{\text{sem}}(x_i, x_j)}{\sum_{l,m} d_{\text{sem}}(x_l, x_m)} \right] \delta(c_i, c_j) \quad (22)$$

For any semantic function  $\mathcal{S}$  with Lipschitz constant  $L_{\mathcal{S}}$ , the  $\epsilon$ -net covering number of the semantic space is bounded by:

$$\mathcal{N}(\epsilon, \mathcal{X}, d_{\text{sem}}) \leq \left( \frac{D}{\epsilon} \right)^d \quad (23)$$

where  $D$  is the diameter of the semantic space and  $d$  is its dimension.

The Personalized PageRank algorithm ensures that sampled nodes provide a  $\delta$ -cover of the semantic space with probability at least  $1 - \delta$  when:

$$|\mathcal{K}_t| \geq \frac{1}{\delta} \left[ d \log \left( \frac{D}{\epsilon} \right) + \log \left( \frac{1}{\delta} \right) \right] \quad (24)$$

Applying the McDiarmid inequality to the empirical semantic distance estimates completes the proof of the high-probability bound.  $\square$

**Corollary 1** (Spectral Approximation Guarantee). *The knowledge encapsulation  $\mathcal{K}t$  provides a  $(\alpha, \beta)$ -spectral approximation of the original graph  $\mathcal{G}$  with high probability, such that:*

$$\alpha \cdot \mathbf{x}^T L_{\mathcal{G}} \mathbf{x} \leq \mathbf{x}^T L_{\mathcal{K}t} \mathbf{x} \leq \beta \cdot \mathbf{x}^T L_{\mathcal{G}} \mathbf{x} \quad \forall \mathbf{x} \in \mathbb{R}^{|\mathcal{V}|} \quad (25)$$

where  $L_{\mathcal{G}}$  and  $L_{\mathcal{K}t}$  are the respective graph Laplacians, and  $\alpha, \beta$  depend on  $|\mathcal{K}_t|$ , the spectral gap of  $\mathcal{G}$ , and the teleportation parameters of the PPR algorithm.

*Proof.* Follows from spectral perturbation theory applied to the effective resistance sampling framework, combined with the properties of Personalized PageRank. The core insight lies in the fact that PPR sampling approximates effective resistance sampling when the teleportation vector is properly calibrated.  $\square$

## A.2 Semantic-Topological Coherence of the Enhancement Agent

We now establish theoretical guarantees for the Enhancement Agent’s generation capabilities, bridging statistical learning theory, concentration inequalities, and manifold theory.

**Definition 2** (Semantic-Topological Coherence). *For a generated node  $v_s$  with attributes  $x_s$  and connections  $\mathcal{E}_s$ , the semantic-topological coherence is defined as:*

$$\Phi(v_s; \mathcal{G}) = \alpha \cdot \mathcal{C}_{\text{sem}}(x_s, \mathcal{X}) + (1 - \alpha) \cdot \mathcal{C}_{\text{topo}}(\mathcal{E}_s, \mathcal{G}) \quad (26)$$

where  $\mathcal{C}_{\text{sem}}$  is semantic coherence,  $\mathcal{C}_{\text{topo}}$  is topological coherence, and  $\alpha \in [0, 1]$  is a weighting parameter.

**Theorem 2** (Generation Consistency with Concentration Bounds). *The Enhancement Agent produces node  $v_s$  with attributes  $x_s$  and edges  $\mathcal{E}_s$  that satisfy:*

1. *Semantic consistency with concentration bounds:*

$$\mathbb{P}(|\mathcal{C}_{\text{sem}}(x_s, \mathcal{X}) - \mathbb{E}[\mathcal{C}_{\text{sem}}(x_s, \mathcal{X})]| > t) \leq 2 \exp \left( -\frac{|\mathcal{K}_t| t^2}{2\sigma_{\text{sem}}^2} \right) \quad (27)$$

2. *Topological consistency with respect to local and global network properties:*

$$\mathbb{E}[\mathcal{C}_{\text{topo}}(\mathcal{E}_s, \mathcal{G})] \geq \beta \cdot \max_{v_j \in \mathcal{V}_k} \mathcal{C}_{\text{topo}}(\mathcal{E}_j, \mathcal{G}) - \frac{C_{\mathcal{G}}}{|\mathcal{K}_t|^{1/3}} \quad (28)$$

3. *The generative mechanism preserves manifold structure in the asymptotic limit:*

$$\lim_{|\mathcal{K}_t| \rightarrow \infty} \mathbb{P}(\text{dist}(x_s, \mathcal{M}_{\mathcal{X}}) > \epsilon) = 0 \quad (29)$$

where  $\mathcal{M}_{\mathcal{X}}$  is the manifold on which the original node attributes lie.

**Proof. Part 1: Semantic Consistency Concentration**

The Enhancement Agent generates node attributes via a conditional autoregressive model:

$$P(x_s | \mathcal{K}_t, \mathcal{R}_t) = \prod_{i=1}^L P(x_s^i | x_s^{<i}, \mathcal{X}_k, \mathcal{E}_k, \mathcal{R}_t) \quad (30)$$

Each token generation can be decomposed as:

$$P(x_s^i | x_s^{<i}, \mathcal{X}_k, \mathcal{E}_k, \mathcal{R}_t) \propto \exp\left(\frac{\phi(x_s^i)^T \mathbf{h}_i}{\tau}\right) \quad (31)$$

where  $\mathbf{h}_i$  is the contextualized representation and  $\tau$  is a temperature parameter.

The contextualized representation integrates information from the knowledge encapsulation:

$$\mathbf{h}_i = \mathbf{W}_1 \cdot f(x_s^{<i}) + \mathbf{W}_2 \cdot g(\mathcal{X}_k) + \mathbf{W}_3 \cdot h(\mathcal{E}_k) \quad (32)$$

Let  $\mathcal{C}_{\text{sem}}(x_s, \mathcal{X}) = \max_{x_j \in \mathcal{X}} \mathcal{S}(x_s, x_j)$ . The semantic similarity function  $\mathcal{S}$  satisfies the bounded differences condition:

$$|\mathcal{S}(x_s, x_j) - \mathcal{S}(x_s, x_{j'})| \leq L_{\mathcal{S}} \cdot |x_j - x_{j'}| \quad (33)$$

By applying McDiarmid's inequality to the empirical semantic coherence, we establish the concentration bounds.

**Part 2: Topological Consistency**

The edge generation mechanism:

$$P((v_s, v_i) \in \mathcal{E}_c | \mathcal{K}_t, \mathcal{R}_t) = \sigma\left(\theta_1 \cdot \text{sim}(x_s, x_i) + \theta_2 \cdot \frac{|\mathcal{N}(v_i) \cap \mathcal{N}_K(v_s)|}{|\mathcal{N}_K(v_s)|} + \theta_3 \cdot \frac{k_i}{\max_j k_j}\right) \quad (34)$$

We analyze the asymptotic properties using random graph theory. Let  $G(n, p_{ij})$  be a random graph model where edge  $(i, j)$  exists with probability  $p_{ij}$ .

The expected clustering coefficient:

$$\mathbb{E}[CC(v_s)] = \frac{\sum_{i,j} p_{is} \cdot p_{js} \cdot p_{ij}}{\sum_{i,j} p_{is} \cdot p_{js}} \quad (35)$$

For our model:

$$p_{ij} = \sigma\left(\theta_1 \cdot \text{sim}(x_i, x_j) + \theta_2 \cdot \frac{|\mathcal{N}(v_i) \cap \mathcal{N}(v_j)|}{|\mathcal{N}(v_i)|} + \theta_3 \cdot \frac{k_j}{\max_l k_l}\right) \quad (36)$$

The local-global consistency emerges from the balance between the three terms:

- $\theta_1$  term preserves homophily (similar nodes connect)
- $\theta_2$  term ensures triadic closure (friends of friends connect)
- $\theta_3$  term maintains scale-free properties (preferential attachment)

Using graph limit theory, the topological consistency is governed by:

$$\mathcal{C}_{\text{topo}}(\mathcal{E}_s, \mathcal{G}) \approx 1 - \frac{1}{2} |W_{\mathcal{E}_s} - W_{\mathcal{G}}|_{\square} \quad (37)$$

where  $W_{\mathcal{E}_s}$  and  $W_{\mathcal{G}}$  are graphons (limiting objects of graphs) and  $|\cdot|_{\square}$  is the cut norm.

### Part 3: Manifold Preservation

Let  $\mathcal{M}_{\mathcal{X}} \subset \mathbb{R}^d$  be a compact  $r$ -dimensional manifold with condition number  $1/\tau$  and reach at least  $\tau > 0$ . The nodes  $\mathcal{X} = x_1, \dots, x_N$  are sampled from a distribution supported on  $\mathcal{M}_{\mathcal{X}}$ .

The language model learns a conditional distribution:

$$P_{\text{LLM}}(x|\mathcal{K}_t) = \frac{1}{Z(\mathcal{K}_t)} \exp\left(-\frac{\text{dist}(x, \mathcal{M}_{\mathcal{X}}(\mathcal{K}_t))^2}{2\sigma^2}\right) \cdot P_{\text{prior}}(x) \quad (38)$$

As  $|\mathcal{K}_t| \rightarrow \infty$ , we have:

$$\mathcal{M}_{\mathcal{X}}(\mathcal{K}_t) \rightarrow \mathcal{M}_{\mathcal{X}} \text{ in the Hausdorff metric} \quad (39)$$

The manifold preservation follows from the consistency of kernel density estimators on manifolds and the properties of autoregressive language models.  $\square$

**Proposition 1** (Latent Variable Interpretation). *The Enhancement Agent’s generative process is equivalent to a controlled stochastic differential equation on the graph manifold:*

$$dx_t = \mu(x_t, \mathcal{K}_t)dt + \sigma(x_t, \mathcal{K}_t)dW_t \quad (40)$$

where  $\mu$  is a drift term aligning generation with the knowledge encapsulation,  $\sigma$  is a diffusion term controlling diversity, and  $W_t$  is a Wiener process.

*Proof.* We establish the equivalence by showing that the discrete token generation process converges to the SDE in the continuous limit. The proof uses techniques from the theory of diffusion models and score-matching generative models.  $\square$

### A.3 Theoretical Properties of Quality Assessment and Convergence

We now establish rigorous guarantees for the Evaluation Agent’s quality assessment and convergence determination capabilities.

**Definition 3** (Marginal Quality Contribution). *For a graph  $\mathcal{G} = (\mathcal{V}, \mathcal{E}, \mathcal{X}, \mathcal{Y})$  and a generated node  $v_s$  with attributes  $x_s$  and connections  $\mathcal{E}_s$ , the marginal quality contribution is:*

$$\Delta Q(v_s, \mathcal{G}) = Q(\mathcal{G} \cup \{v_s, \mathcal{E}_s\}) - Q(\mathcal{G}) \quad (41)$$

where  $Q$  is a quality functional measuring overall graph utility for the target task.

**Theorem 3** (Quality Assessment with Statistical Guarantees). *The Evaluation Agent implements a quality assessment function that satisfies:*

1. *Strong correlation with marginal quality contribution:*

$$\mathbb{E}[\Delta Q(v_s, \mathcal{G}) | \text{LLM}_{\mathcal{V}}(v_s, \mathcal{R}_0, \mathcal{R}_t, \mathcal{K}_t) = q] = f(q) + O\left(\frac{1}{|\mathcal{V}|}\right) \quad (42)$$

where  $f$  is monotonically increasing and Lipschitz continuous.

2. *Thresholding efficiency with probabilistic guarantees:*

$$\mathbb{P}(\Delta Q(v_s, \mathcal{G}) > 0 | \text{LLM}_{\mathcal{V}}(v_s, \mathcal{R}_0, \mathcal{R}_t, \mathcal{K}_t) > \tau_t) \geq 1 - \exp(-c \cdot |\mathcal{K}_t|) \quad (43)$$

for some constant  $c > 0$  and appropriately chosen threshold  $\tau_t$ .

3. *Convergence detection with statistical significance:*

$$\mathbb{P}(\text{Converged}_t = 1 | \mathbb{E}[\Delta Q_{t+1}] < \epsilon) \geq 1 - \delta \quad (44)$$

where  $\delta$  decreases exponentially with the window size  $k$  in the convergence criterion.

*Proof. Part 1: Correlation with Marginal Quality*

The Evaluation Agent employs a multi-dimensional quality assessment:

$$\text{LLM}_{\mathcal{V}}(v_s, \mathcal{R}_0, \mathcal{R}_t, \mathcal{K}_t) = g(\Phi_{\text{sem}}(v_s, \mathcal{K}_t), \Phi_{\text{topo}}(v_s, \mathcal{G}_t), \Phi_{\text{bal}}(v_s, \mathcal{Y}_t)) \quad (45)$$



The quality functional  $Q$  can be decomposed into semantic, topological, and balance components:

$$Q(\mathcal{G}) = \omega_1 Q_{\text{sem}}(\mathcal{G}) + \omega_2 Q_{\text{topo}}(\mathcal{G}) + \omega_3 Q_{\text{bal}}(\mathcal{G}) \quad (46)$$

For each component, we establish bounds on the approximation error:

$$|\mathbb{E}[\Delta Q_{\text{sem}}(v_s, \mathcal{G}) \mid \Phi_{\text{sem}}(v_s, \mathcal{K}t) = s] - f_{\text{sem}}(s)| \leq \frac{C_1}{|\mathcal{K}t|} \quad (47)$$

$$|\mathbb{E}[\Delta Q_{\text{topo}}(v_s, \mathcal{G}) \mid \Phi_{\text{topo}}(v_s, \mathcal{G}t) = t] - f_{\text{topo}}(t)| \leq \frac{C_2}{|\mathcal{V}|} \quad (48)$$

$$|\mathbb{E}[\Delta Q_{\text{bal}}(v_s, \mathcal{G}) \mid \Phi_{\text{bal}}(v_s, \mathcal{Y}t) = b] - f_{\text{bal}}(b)| \leq \frac{C_3}{\sqrt{|\mathcal{V}|}} \quad (49)$$

By the properties of the LLM's function approximation capabilities, we have:

$$\|g - \omega_1 f_{\text{sem}} - \omega_2 f_{\text{topo}} - \omega_3 f_{\text{bal}}\|_{\infty} \leq \epsilon_{\text{LLM}} \quad (50)$$

Combining these bounds establishes the correlation with marginal quality.

### Part 2: Thresholding Efficiency

The adaptive threshold mechanism:

$$\tau_t = \tau_{t-1} + \zeta(\bar{\mathcal{F}}_t(\omega_t^*) - \bar{\mathcal{F}}_{t-1}(\omega_{t-1}^*)) \quad (51)$$

converges to an optimal threshold  $\tau^*$  that maximizes expected improvement:

$$\tau^* = \arg \max_{\tau} \mathbb{E}[\Delta Q(\mathcal{V}_{\text{accepted}}(\tau), \mathcal{G})] \quad (52)$$

where  $\mathcal{V}_{\text{accepted}}(\tau) = v_s : \text{LLM}_V(v_s, \cdot) > \tau$ .

By the properties of sub-Gaussian random variables and the Lipschitz continuity of  $f$ , we establish the high-probability guarantee on positive quality contribution.

### Part 3: Convergence Detection

The convergence criterion:

$$\text{Converged}_t = \mathbb{I} \left( \max_{j \in \{1, \dots, k\}} |\bar{\mathcal{F}}_t(\omega_t^*) - \bar{\mathcal{F}}_{t-j}(\omega_{t-j}^*)| < \epsilon \wedge \text{LLM}_{\text{goal}}(\mathcal{R}_0, \mathcal{R}_t) = \text{True} \right) \quad (53)$$

implements a change-point detection algorithm with multiple hypothesis testing.

The probability of false convergence detection is bounded by:

$$\mathbb{P}(\text{Converged}_t = 1 \mid \mathbb{E}[\Delta Q_{t+1}] \geq \epsilon) \leq k \cdot \exp \left( -\frac{2n\epsilon^2}{C_Q^2} \right) \quad (54)$$

where  $n$  is the number of samples used to estimate  $\bar{\mathcal{F}}_t$  and  $C_Q$  is a bound on the quality range.

Likewise, the probability of missing convergence is bounded by:

$$\mathbb{P}(\text{Converged}_t = 0 \mid \mathbb{E}[\Delta Q_{t+1}] < \epsilon/2) \leq \exp \left( -\frac{n\epsilon^2}{8C_Q^2} \right) \quad (55)$$

The combined error probability decays exponentially with the sample size and window length.  $\square$

**Corollary 2** (Optimal Stopping Property). *The Evaluation Agent's convergence criterion implements an approximately optimal stopping rule for the synthesis process, achieving a regret bound of:*

$$\text{Regret}(T) \leq O \left( \sqrt{T \log T} \right) \quad (56)$$

where  $T$  is the maximum number of iterations.

*Proof.* We frame the convergence determination as a multi-armed bandit problem with non-stationary rewards, where the arms correspond to continue/stop decisions. Applying results from optimal stopping theory and the regret analysis of UCB algorithms yields the result.  $\square$

#### A.4 Unified Multi-Agent System Dynamics

We now establish theoretical results concerning the collective behavior of the agent system, framing it as optimization on a Riemannian manifold.

**Definition 4** (Graph Configuration Manifold). *The space of possible graph configurations forms a Riemannian manifold  $\mathcal{M}_{\mathcal{G}}$  with metric tensor:*

$$g_{ij}(\mathcal{G}) = \mathbb{E} \left[ \frac{\partial \log p(\mathcal{G}|\theta)}{\partial \theta_i} \frac{\partial \log p(\mathcal{G}|\theta)}{\partial \theta_j} \right] \quad (57)$$

where  $p(\mathcal{G}|\theta)$  is a parametric model of graph distribution and  $\theta$  are the parameters.

**Theorem 4** (Manifold Optimization Dynamics). *The multi-agent system in GraphMaster implements natural gradient ascent on the graph configuration manifold  $\mathcal{M}_{\mathcal{G}}$ , optimizing a multi-objective function:*

$$\Psi^*(\mathcal{G}) = \lambda_1 \Psi_{sem}(\mathcal{G}) + \lambda_2 \Psi_{struct}(\mathcal{G}) + \lambda_3 \Psi_{bal}(\mathcal{G}) \quad (58)$$

with adaptive weights  $\lambda_i$  that evolve according to:

$$\lambda_i^{t+1} = \Pi_{\Delta} [\lambda_i^t + \eta \nabla_{\lambda_i} P(\mathcal{G}_t)] \quad (59)$$

where  $\Pi_{\Delta}$  is projection onto the probability simplex.

The convergence rate is:

$$\mathbb{E}[\Psi^*(\mathcal{G}^*) - \Psi^*(\mathcal{G}_T)] \leq O\left(\frac{1}{\sqrt{T}}\right) \quad (60)$$

for a non-convex objective, and:

$$\mathbb{E}[\Psi^*(\mathcal{G}^*) - \Psi^*(\mathcal{G}_T)] \leq O\left(\frac{\log T}{T}\right) \quad (61)$$

if the objective satisfies Polyak-Łojasiewicz conditions.

##### Proof. Part 1: Natural Gradient Dynamics

At each iteration, the system performs:

$$\mathcal{G}_{t+1} = \Pi_{\mathcal{M}_{\mathcal{G}}} [\mathcal{G}_t + \eta_t \cdot \mathcal{I}^{-1}(\mathcal{G}_t) \cdot \nabla \Psi^*(\mathcal{G}_t)] \quad (62)$$

where  $\mathcal{I}(\mathcal{G}_t)$  is the Fisher information matrix and  $\Pi_{\mathcal{M}_{\mathcal{G}}}$  is projection onto the manifold.

This update is implemented by the collaborative agent process:

$$\mathcal{K}_t = \Phi(\mathcal{G}_t) \quad (63)$$

$$\mathcal{V}_s^t = \text{LLM}_E(\mathcal{K}_t, \mathcal{R}_t, M_t) \quad (64)$$

$$\mathcal{E}_s^t = \{(v_s, v_i) \mid P((v_s, v_i) \mid \mathcal{K}_t, \mathcal{R}_t) > \eta_t\} \quad (65)$$

$$\mathcal{V}_{\text{accepted}}^t = \{v_s \in \mathcal{V}_s^t \mid \text{LLM}_V(v_s, \mathcal{R}_0, \mathcal{R}_t, \mathcal{K}_t) > \tau_t\} \quad (66)$$

$$\mathcal{G}_{t+1} = \mathcal{G}_t \oplus \left( \mathcal{V}_{\text{accepted}}^t, \mathcal{E}_s^t \Big|_{\mathcal{V}_{\text{accepted}}^t} \right) \quad (67)$$

##### Part 2: Adaptive Weight Dynamics

The Manager Agent implements online gradient-based multi-objective optimization:

$$\lambda_i^{t+1} = \Pi_{\Delta} [\lambda_i^t + \eta \nabla_{\lambda_i} P(\mathcal{G}_t)] \quad (68)$$

where  $P(\mathcal{G}_t)$  measures progress toward synthesis objectives.

This follows the Multiple Gradient Descent Algorithm (MGDA) for Pareto optimization:

$$\nabla_{\lambda_i} P(\mathcal{G}_t) \approx \nabla_{\lambda_i} \min_j \frac{\Psi_j(\mathcal{G}_t) - \Psi_j(\mathcal{G}_0)}{\Psi_j^* - \Psi_j(\mathcal{G}_0)} \quad (69)$$

##### Part 3: Convergence Analysis

For a general non-convex objective, we have:

$$\mathbb{E} \left[ \min_{t=0,1,\dots,T-1} |\nabla \Psi^*(\mathcal{G}_t)|^2 \right] \leq \frac{2[\Psi^*(\mathcal{G}^*) - \Psi^*(\mathcal{G}_0)]}{\eta T} + \frac{\eta L}{2} \quad (70)$$

For appropriately chosen step size  $\eta = O(1/\sqrt{T})$ , this yields the  $O(1/\sqrt{T})$  convergence rate.

If the objective satisfies the Polyak-Łojasiewicz condition:

$$|\nabla \Psi^*(\mathcal{G})|^2 \geq 2\mu[\Psi^*(\mathcal{G}^*) - \Psi^*(\mathcal{G})] \quad (71)$$

for some  $\mu > 0$ , then we obtain the improved  $O(\frac{\log T}{T})$  rate.  $\square$

**Theorem 5** (Spectral Convergence of Synthesized Graphs). *Let  $\mathcal{G}_{orig}$  be the original graph and  $\mathcal{G}_{synth}$  be the synthesized graph after convergence. Under appropriate conditions on the synthesis process, the eigenvalue distributions of their normalized Laplacians converge:*

$$\lim_{|\mathcal{V}| \rightarrow \infty} d_{LP}(\rho_{\mathcal{G}_{orig}}, \rho_{\mathcal{G}_{synth}}) = 0 \quad (72)$$

where  $d_{LP}$  is the Lévy-Prokhorov metric between spectral distributions and  $\rho_{\mathcal{G}}$  is the empirical spectral distribution of graph  $\mathcal{G}$ .

*Proof.* We establish this result by analyzing the perturbation of the graph spectrum under node additions. The proof relies on matrix concentration inequalities and recent results in random matrix theory concerning deformed Wigner matrices.

For graphs with bounded degree, the spectral distribution satisfies a semicircle law in the limit. The synthesis process preserves this property through controlled edge formation that maintains degree distribution and local clustering patterns.  $\square$

These theoretical results collectively establish the mathematical foundations underlying GraphMaster’s effectiveness, providing formal guarantees for its information preservation, generation quality, evaluation accuracy, and convergence properties. The integration of concepts from information theory, statistical learning, manifold optimization, and spectral graph theory creates a comprehensive theoretical framework that explains why our multi-agent approach succeeds in generating high-quality text-attributed graphs in data-limited environments.

## B Detailed comparison between GraphMaster and GAG

We’ve found that while the recent GAG framework [17] has made breakthroughs in social network simulation, it differs fundamentally from our work. GAG primarily focuses on generating large-scale social networks through user-item interactions, excelling at simulating macroscopic properties like small-world phenomena and power-law distributions. It builds networks through interactions between homogeneous “actor” agents and can indeed handle graphs with hundreds of thousands of nodes, but its goals differ significantly from ours. In contrast, we designed GraphMaster specifically to address text-attributed graph (TAG) synthesis in data-scarce environments. We’ve adopted a more targeted approach—combining four distinct LLM agents (Manager, Perception, Enhancement, and Evaluation), each with specialized roles. This division of labor allows us to simultaneously tackle the two most challenging aspects of TAG synthesis: semantic coherence of textual nodes and structural integrity of the graph.

GraphMaster’s most distinctive feature is its iterative refinement mechanism. The Evaluation agent continuously examines newly generated graph elements, filtering high-quality content based on semantic and topological criteria. This process is guided by a multi-objective optimization function:

$$\omega_t^* = \arg \max_{\omega \in \Omega} [\lambda_1 U_{\text{sem}}(\omega, G_t) + \lambda_2 U_{\text{struct}}(\omega, G_t) + \lambda_3 U_{\text{bal}}(\omega, G_t)], \quad (73)$$

This ensures we achieve an optimal balance between semantic coherence, structural accuracy, and class balance.

Another important difference lies in how we address LLM limitations. To solve context window constraints, we’ve developed techniques like community-based sampling and personalized PageRank to effectively extract the most representative subgraphs as context. GAG, however, employs more generic agent interactions and parallel simulations without specifically focusing on semantic consistency at the node attribute level. Overall, while GAG demonstrates excellence in large-scale social network simulation, GraphMaster provides a more specialized and reliable framework for high-quality TAG synthesis in data-constrained environments. This makes GraphMaster particularly suitable for advancing Graph Foundation Models (GFMs) in data-scarce scenarios.

## C The implement details of newly created baseline

### C.1 Mixed-LLM

Mixed-LLM introduces a novel interpolative synthesis approach that extends the seminal mixup concept from computer vision to text-attributed graphs via large language models. This method operates on the principle of manifold-aware semantic interpolation, where node representations from different classes are strategically combined to generate semantically coherent yet diverse synthetic nodes.

The Mixed-LLM algorithm consists of three primary phases:

1. **Strategic Class-Balanced Sampling:** Rather than random selection, Mixed-LLM employs a distribution-aware sampling strategy:

$$S = \{(v_i, y_i) | v_i \in V, P(v_i) \propto 1/|V_{y_i}|^\alpha\} \quad (74)$$

where  $\alpha$  is an adaptive parameter controlling the emphasis on minority classes and  $|V_{y_i}|$  represents the cardinality of nodes with label  $y_i$ .

2. **Latent Space Interpolation:** For each pair of sampled nodes  $(v_i, v_j)$ , Mixed-LLM generates a convex combination in the semantic space:

$$\tilde{x}_s = \lambda \cdot \phi_{LLM}(x_i) + (1 - \lambda) \cdot \phi_{LLM}(x_j) \quad (75)$$

where  $\phi_{LLM}$  represents the LLM’s latent representation function and  $\lambda \sim \text{Beta}(\alpha, \alpha)$  is a mixing coefficient.

3. **LLM-Guided Textual Manifestation:** The interpolated representation is transformed into coherent textual attributes through a prompt-based generation:

$$x_s = \text{LLM}_M(p(\tilde{x}_s, x_i, x_j, y_i, y_j)) \quad (76)$$

where  $p$  is a carefully designed prompt template instructing the LLM to create textual attributes that preserve the semantic characteristics of both source nodes while maintaining linguistic naturalness.

The final label assignment follows a soft probability distribution:

$$P(y_s = c) = \lambda \cdot I[y_i = c] + (1 - \lambda) \cdot I[y_j = c] \quad (77)$$

where  $I$  is the indicator function. This probabilistic formulation enables Mixed-LLM to generate boundary-enhancing examples that improve classifier robustness.

### C.2 Synthesis-LLM

Synthesis-LLM implements a context-aware graph sampling and generative synthesis framework that leverages structural locality principles to inform LLM-based node generation. Unlike conventional approaches that process graph data indiscriminately, Synthesis-LLM employs sophisticated topological sampling to create representative subgraph contexts that maximize information density within LLM token constraints.

The framework operates in four sequential stages:

1. **Multi-strategy Subgraph Sampling:** Synthesis-LLM employs a hybrid sampling approach that combines Personalized PageRank (PPR) with strategic breadth-first search:

$$K_s = \Gamma_{PPR}(G, v_s, \alpha, r) \cup \Gamma_{BFS}(G, v_s, d) \quad (78)$$

where  $\Gamma_{PPR}$  samples nodes based on their PPR scores from seed node  $v_s$  with damping factor  $\alpha$  and threshold  $r$ , while  $\Gamma_{BFS}$  complements this with a depth-limited breadth-first expansion to depth  $d$ .

2. **Structural-Semantic Context Formulation:** The sampled subgraph is transformed into a rich prompt context:

$$C = f_{context}(K_s, A[K_s], X[K_s]) \quad (79)$$

where  $f_{context}$  is a specialized function that encodes both topological relationships and textual attributes into a structured prompt format.

3. **Guided Generative Synthesis:** The LLM generates new nodes conditioned on the extracted context:

$$(x_s, E_s) = \text{LLM}_S(C, \theta) \quad (80)$$

where  $\text{LLM}_S$  represents the synthesis LLM with temperature parameter  $\theta$  that balances creativity and fidelity.

4. **Structural Consistency Enforcement:** Generated nodes undergo topological validation to ensure adherence to the original graph’s structural patterns:

$$E'_s = \{e \in E_s | P_{structure}(e|G) > \tau\} \quad (81)$$

where  $P_{structure}$  estimates the probability of edge  $e$  existing given the structural patterns in  $G$ , and  $\tau$  is an acceptance threshold.

This methodology enables Synthesis-LLM to generate nodes that maintain both semantic relevance and structural coherence with respect to the original graph, while requiring minimal examples due to the LLM’s inherent understanding of semantic relationships.

### C.3 Experimental details

We selected QwQ-32B [29] as the large language model for these two baselines, and used two A6000 GPUs with 48G memory for the experiments.

#### C.3.1 Hyperparameter Selection for Mixed-LLM

In Mixed-LLM, extensive grid search and ablation studies were conducted to optimize key hyperparameters. The class balancing parameter  $\alpha$  was tuned within the range [0.5, 1.5] with an optimal value of 0.8, ensuring a good balance between preserving the original class distribution and addressing class imbalance issues. The beta distribution parameter for the mixing coefficient, where  $\lambda \sim \text{Beta}(\alpha, \alpha)$ , achieved optimal performance at 0.4, producing meaningful boundary examples. Additionally, an LLM temperature of 0.7 provided the best balance between creative variation and semantic consistency, and incorporating 2–3 example interpolations in the prompt significantly enhanced generation quality.

#### C.3.2 Hyperparameter Selection for Synthesis-LLM

For Synthesis-LLM, the hyperparameters were optimized to capture both local and global graph structures. A PPR damping factor  $\alpha$  of 0.65 offered a suitable trade-off between local neighborhood exploration and distant node influence, while a PPR threshold  $r = 0.005$  effectively identified relevant nodes. A BFS depth limit of  $d = 2$  was sufficient to extract essential structural context without overloading the LLM’s input. Moreover, setting the generation temperature  $\theta$  to 0.5 ensured structural and semantic coherence, and a structural acceptance threshold  $\tau$  of 0.6 successfully filtered edge proposals. Overall, the optimal performance was achieved when 25–35 representative nodes were included in the LLM context.

## D Data-limited Datasets Creation

To simulate realistic scenarios where annotated data is scarce, we generate data-limited datasets by extracting carefully curated subgraphs from the original large-scale graphs. Our procedure begins by partitioning the original graph based on node labels and inherent manifold properties, ensuring that the semantic distribution and community structures are preserved. Next, we apply a multi-objective sampling strategy that leverages node degrees, community representation, and bridge node potentials to select a subset of nodes and their associated edges. This approach, outlined in Algorithm 1, is designed to maintain the essential connectivity patterns and spectral features of the full graph while significantly reducing the number of nodes. Iterative refinements are then performed to balance class proportions and correct any topological distortions, resulting in a smaller yet representative subgraph that closely mimics the original graph’s structure and attribute distribution. This data-limited setup provides a robust testbed for evaluating the effectiveness of our graph synthesis methods under constrained conditions.

## E Statistics of the Datasets

Table 3 shows the basic characteristics of our new synthesized dataset. We introduce our dataset from seven aspects: Nodes, Edges, Classes, Louvain communities, Training nodes, Validation nodes and Test nodes, including the original dataset and our newly generated Data-limited dataset.

## F Hyperparameter Sensitivity Analysis

In this section, we examine how different hyperparameter settings affect the performance and synthesis quality of our proposed GraphMaster framework. We consider a comprehensive set of hyperparameters controlling the sample size, node generation proportion, semantic and structural balancing, stochastic exploration, quality thresholds, and convergence criteria. Our experimental results indicate that GraphMaster is robust to moderate variations in these parameters, with the most sensitive being the edge formation coefficients  $(\theta_1, \theta_2, \theta_3)$  and the quality threshold  $\tau$ . Based on extensive experiments on multiple text-attributed graph datasets, we recommend a default configuration comprising

**Algorithm 1**  $\mathcal{M}$ -Preserving Graph Sampling**Require:** Graph  $G = (V, E, \mathcal{X}, \mathcal{Y}, \mathcal{M})$ , sampling ratio  $\alpha \in (0, 1]$ , convergence threshold  $\epsilon$ **Ensure:** Homeomorphic sampled graph  $G_s$  preserving manifold properties

- 1:  $\Phi_G \leftarrow \mathcal{T}(G)$  ▷ Extract property tensor capturing distributions and spectral features
- 2:  $\mathcal{C} \leftarrow \arg \max_{\mathcal{C}'} \mathcal{Q}(\mathcal{C}', G)$  ▷ Optimize modularity for community detection
- 3:  $\mathcal{D} \leftarrow \{V_{y,m}\}_{y,m}$  where  $V_{y,m} = \{v \in V : \mathcal{Y}(v) = y, \mathcal{M}(v) = m\}$  ▷ Create attribute partitions
- 4:  $\Pi \leftarrow \{\pi_{y,m} = |V_{y,m}|/|V|\}_{y,m}$  ▷ Joint distribution tensor
- 5:  $\mathbf{K} \leftarrow \lfloor |V| \cdot \alpha \cdot \Pi \rfloor$  ▷ Target counts per partition
- 6:  $\mathbf{K} \leftarrow \mathbf{K} + \delta(\mathbf{K}, \alpha|V|)$  ▷ Correct sampling counts to exactly match target size
- 7:  $V_s \leftarrow \emptyset$  ▷ Initialize sampled node set
- 8: **for**  $(y, m) \in \{(\mathcal{Y}, \mathcal{M})\}$  **do**
- 9:   **if**  $|V_{y,m}| \leq \mathbf{K}_{y,m}$  **then**
- 10:      $V_s \leftarrow V_s \cup V_{y,m}$
- 11:   **else**
- 12:      $\Omega_{y,m} \leftarrow$  Multi-objective weight vector where for each  $v \in V_{y,m}$ :

$$\Omega_{y,m}(v) = \lambda_1 \frac{\deg(v)}{\max_u \deg(u)} + \lambda_2 \left(1 - \frac{|V_s \cap \mathcal{C}(v)|}{|\mathcal{C}(v)|}\right) + \lambda_3 \beta_{\text{bridge}}(v) \quad (82)$$

- 13:      $V_s \leftarrow V_s \cup \text{TopK}(V_{y,m}, \Omega_{y,m}, \mathbf{K}_{y,m})$
- 14:   **end if**
- 15: **end for**
- 16:  $G'_s \leftarrow G[V_s]$  ▷ Initial induced subgraph
- 17: **if**  $\|\kappa(G'_s) - \kappa(G)\| > \epsilon$  **then** ▷ Check connectivity distortion
- 18:    $\mathcal{B} \leftarrow$  Bridge nodes  $(V \setminus V_s)$  sorted by connectivity gain potential
- 19:    $\mathcal{R} \leftarrow$  Replaceable nodes in  $V_s$  with minimal structural impact
- 20:   **while**  $\|\kappa(G'_s) - \kappa(G)\| > \epsilon$  and  $\mathcal{B} \neq \emptyset$  and  $\mathcal{R} \neq \emptyset$  **do**
- 21:      $(b^*, r^*) \leftarrow \arg \max_{b \in \mathcal{B}, r \in \mathcal{R}} \mathcal{S}(b, r)$  subject to  $\mathcal{Y}(b) = \mathcal{Y}(r) \wedge \mathcal{M}(b) = \mathcal{M}(r)$
- 22:      $V_s \leftarrow (V_s \setminus \{r^*\}) \cup \{b^*\}$
- 23:      $G'_s \leftarrow G[V_s]$
- 24:     Update  $\mathcal{B}, \mathcal{R}$
- 25:   **end while**
- 26: **end if**
- 27: **return**  $G'_s$

Table 3: Dataset Statistics

Dataset	# Nodes	# Edges	# Classes	# Louvain communities	# Training nodes	# Validation nodes	# Test nodes
Cora	2708	5278	7	106	1624	542	542
Citeseer	3186	4225	6	506	1911	637	638
Wikics	8196	104161	10	540	580	1769	5847
History	41551	251590	12	2036	24921	8337	8293
Arxiv2023	46198	38863	38	28901	28905	27718	9240
Children	76875	1162522	24	2296	46010	15455	15410
SubCora	1354	2486	7	99	815	267	272
SubCiteseer	1274	1360	6	486	764	255	255
SubWikics	1639	26786	10	374	111	350	1178
SubHistory	2077	40415	12	17	1249	416	412
SubArxiv2023	2309	3119	38	1407	1398	456	455
SubChildren	3843	94636	24	71	2308	766	769

a sample size of  $N = 30$  and a new node percentage  $M\%$  between 10% and 20%. Furthermore, setting  $\mu = 0.5$ ,  $\gamma = 0.5$ , and  $\beta = 2.0$  is advised, while the edge probability coefficients should be either adaptively tuned or fixed according to the specific enhancement mode. We further determine that a fixed initial threshold  $\tau_0 = 7.0$  with an adaptive update rate  $\zeta = 0.1$  and a convergence threshold  $\epsilon = 0.05$  yield optimal performance. Finally, initializing the adaptive weights as  $\lambda_{\text{sem}} = \lambda_{\text{struct}} = \lambda_{\text{bal}} = 0.33$  and employing a learning rate  $\eta = 0.05$  provides a favorable balance between performance, generation quality, and computational efficiency. In the following subsections, we detail the sensitivity analysis for each hyperparameter, offering practical guidelines for configuring GraphMaster in diverse scenarios.

### F.1 Sample Size ( $N$ ) and New Node Percentage ( $M\%$ )

The **sample size** ( $N$ ) determines how many background nodes are selected for the knowledge extraction step, while the **new node percentage** ( $M\%$ ) specifies the fraction of newly generated nodes relative to the extracted background knowledge. Empirically, we find that:

- Performance steadily improves when  $N$  increases from 10 to 30, as the richer context benefits downstream tasks.
- Beyond  $N = 40$ , additional background nodes cause diminishing returns and potential performance drops on certain datasets, likely due to noise introduced by excessive context.
- For  $M\%$ , performance typically peaks around 15%. If  $M\%$  is too low (1%-10%), not enough new semantic content is introduced. Conversely, higher percentages (20%-30%) can degrade node quality since the model must generate excessive content at once.

Based on these observations, we recommend  $N \approx 30$  and  $M \in [10, 20]\%$  for a balanced trade-off between context richness and generation overhead.

### F.2 Semantic Variance Weight ( $\mu$ )

The parameter  $\mu$  controls the relative importance of *semantic variance* in community selection when running in semantic enhancement mode. We vary  $\mu \in [0.1, 1.0]$  and observe that  $\mu = 0.5$  consistently yields the best performance. Lower  $\mu$  values ( $< 0.3$ ) favor large communities regardless of semantic cohesion, while higher values ( $> 0.7$ ) overemphasize variance and may cause the selection of overly small, semantically disjoint communities. Balancing both community size and semantic diversity is essential for high-quality text generation.

### F.3 Modularity Balance ( $\gamma$ )

In semantic-enriched modularity maximization, the parameter  $\gamma$  governs the balance between structural and semantic factors. We explore  $\gamma \in [0, 1]$ :

- $\gamma = 0.0$  corresponds to a purely semantic-based community detection that can overlook critical structural features.
- $\gamma = 1.0$  corresponds to traditional structure-based detection, which disregards semantic context.
- Intermediate values ( $\gamma = 0.5$  to  $0.7$ ) consistently produce superior performance. This sweet spot reflects the complementary roles of text semantics and graph structure in forming coherent communities.

Moreover, slightly lower  $\gamma$  values (e.g., 0.4) appear more suitable for citation networks, whereas social networks tend to benefit from slightly higher settings (e.g., 0.6 to 0.7).

### F.4 Stochasticity Control ( $\beta$ )

During the hierarchical stochastic diffusion sampling,  $\beta$  controls the degree of random exploration:

- Lower  $\beta$  values ( $< 1.5$ ) make node selection almost deterministic, which can limit the diversity of the sampled subgraph.
- Higher  $\beta$  values ( $> 2.5$ ) can lead to excessive randomness, incorporating nodes only marginally relevant to the query focus.
- Across diverse datasets,  $\beta = 2.0$  provides the best balance between exploration and exploitation.

### F.5 Edge Probability Coefficients ( $\theta_1, \theta_2, \theta_3$ )

We implement an edge probability model for linking new nodes:

$$P((v_s, v_i) \in E) = \sigma\left(\theta_1 \cdot \text{sim}(x_s, x_i) + \theta_2 \cdot \frac{|N(v_i) \cap N_K(v_s)|}{|N_K(v_s)|} + \theta_3 \cdot \frac{k_i}{\max_j k_j}\right), \quad (83)$$

where  $\text{sim}$  is a semantic similarity function, and  $\sigma(\cdot)$  is the sigmoid. In semantic mode, setting  $\theta_1 = 0.6$ ,  $\theta_2 = 0.3$ , and  $\theta_3 = 0.1$  appears optimal, emphasizing textual consistency. In topological mode, the best performance emerges at  $\theta_1 = 0.2$ ,  $\theta_2 = 0.5$ , and  $\theta_3 = 0.3$ , highlighting neighborhood overlap and degree centrality. Notably, allowing  $\theta$ -parameters to adapt automatically to graph characteristics outperforms any fixed configuration by about 1.8% on average.

## F.6 Quality Threshold ( $\tau_t$ )

The **acceptance threshold**  $\tau_t$  determines which newly generated nodes meet the minimum quality to be retained:

- Fixed thresholds reveal a trade-off: higher thresholds ( $\tau > 7.5$ ) ensure higher-quality nodes but yield fewer samples, while lower thresholds ( $\tau < 6.5$ ) broaden quantity at the risk of inconsistent node quality.
- In our experiments,  $\tau = 7.0$  is close to the best static choice.

An **adaptive threshold** rule

$$\tau_t = \tau_{t-1} + \zeta (\bar{F}_t(\omega_t^*) - \bar{F}_{t-1}(\omega_{t-1}^*)),$$

with  $\tau_0 = 7.0$  and  $\zeta \in [0.05, 0.1]$ , outperforms fixed thresholds by approximately 2.3%, demonstrating that dynamic quality updates aligned with synthesis progress are beneficial.

## F.7 Convergence Threshold ( $\epsilon$ )

We define  $\epsilon$  as a convergence criterion based on the gradient of the overall quality improvement. Small  $\epsilon$ -values (e.g.,  $< 0.03$ ) prolong synthesis without appreciable gains, whereas large values (e.g.,  $> 0.1$ ) risk early termination. In practice,  $\epsilon = 0.05$  allows enough refinement iterations while avoiding wasted computation. Simpler datasets (Cora, Citeseer) converge in 6–9 iterations, whereas more complex graphs (History, Children) may require 10–16 iterations for optimal synthesis.

## F.8 Adaptive Weights ( $\lambda_{\text{sem}}, \lambda_{\text{struct}}, \lambda_{\text{bal}}$ )

Within GraphMaster, a *multi-objective utility function* balances three primary objectives: semantic coherence, structural integrity, and class balance. Their weights are denoted  $\lambda_{\text{sem}}, \lambda_{\text{struct}}, \lambda_{\text{bal}}$ . We find that initialization at  $\lambda_{\text{sem}} = \lambda_{\text{struct}} = \lambda_{\text{bal}} = 0.33$  generally works well. The agents subsequently adjust these weights during the iterative enhancements, making the final results robust to the specific initial choice. Citation networks tend to increase  $\lambda_{\text{sem}}$  during training, while social networks rely more on  $\lambda_{\text{struct}}$ .

## F.9 Learning Rate ( $\eta$ ) for Adaptive Weights

When updating the adaptive weights, the **learning rate**  $\eta$  affects the speed and stability of convergence. By testing  $\eta \in [0.01, 0.1]$ , we identify  $\eta = 0.05$  as the best balance. Smaller values ( $< 0.03$ ) slow adaptation, while larger values ( $> 0.08$ ) risk weight oscillations that adversely affect performance.

## F.10 Model Choice and Early Stopping

We compare four candidate large language models (QWQ-32B, QWEN-32B, DEEPSEEK-R1-32B, and LLAMA-33B) within the GraphMaster framework and consistently observe that QWQ-32B outperforms the others, likely due to its balanced training on both factual and generative tasks. For *early stopping*, we set a maximum iteration threshold of 10. Fewer than 10 often terminates the synthesis prematurely, and beyond 10–12 seldom provides additional performance gains.

## G Detailed Experimental Results

Table 1 presents the experimental results using the GCN model, Table 4 shows results using the JKNet model, Table 5 displays results using the GraphSage model, and Table 6 demonstrates results using the GAT model. Our findings indicate that GraphMaster consistently outperforms other approaches across all GNN architectures, strongly validating the universality of our proposed model. Furthermore, we observe that our two novel baselines frequently achieve second-place rankings, which substantiates the significant potential of Large Language Models (LLMs) in text-attributed graph data synthesis. As the first work leveraging LLMs for text-attributed graph synthesis, GraphMaster exhibits both efficient resource utilization and remarkable capabilities for TAG data generation.

## H Detailed Graph Feature Analysis

To rigorously evaluate the structural fidelity of our synthesized graphs, we conduct a comprehensive feature analysis across three critical topological and semantic dimensions. Figure 4, Figure 5, Figure 6, Figure 7, Figure 8 and Figure 9



Table 4: Comparison of GraphMaster with other TAG synthesis methods in JKNet model.

Type	Model	Cora		Citeseer		Wikics		History		Arxiv2023		Children	
		Acc	F1	Acc	F1	Acc	F1	Acc	F1	Acc	F1	Acc	F1
Original	Origin	88.9±1.1	87.9±0.7	78.3±0.9	75.7±1.2	79.7±0.6	77.9±1.1	84.2±0.3	43.1±1.3	76.3±0.8	54.9±1.2	52.6±0.5	31.9±0.9
Classic-Aug	GAugO	88.9±0.4	88.2±1.2	78.3±1.4	77.0±0.8	80.0±0.7	77.8±1.0	84.6±1.2	44.7±1.4	76.8±1.0	53.0±1.2	51.8±0.8	33.6±1.4
LLM-Aug	GraphEdit	91.0±1.3	89.4±1.0	81.4±0.7	80.2±0.8	82.0±0.9	80.6±0.7	87.6±1.0	45.7±1.1	78.0±0.4	57.8±1.1	54.3±1.3	35.7±0.4
	LLM4RGNN	91.4±0.9	88.8±0.5	81.0±1.4	76.7±0.7	83.6±0.3	81.4±0.5	88.9±0.8	48.6±1.4	79.3±1.2	59.1±1.4	55.7±0.7	36.7±1.1
Classic-Syn	GraphSmote	88.7±0.4	87.4±0.8	78.2±1.4	74.8±0.9	80.7±0.3	78.5±0.8	84.9±0.8	43.9±1.4	76.2±1.0	55.5±1.3	53.1±0.7	33.2±0.5
	G-Mixup	87.4±1.0	87.0±0.5	78.4±0.3	76.9±1.0	79.7±1.0	78.0±1.3	84.6±1.1	43.6±1.2	76.6±1.2	56.5±0.8	53.0±1.1	33.0±0.3
	IntraMix	80.9±1.4	82.9±1.0	71.4±0.4	70.7±1.4	73.7±1.3	74.4±0.5	82.4±1.3	42.7±0.4	72.4±1.0	53.9±1.2	45.2±1.0	30.1±0.5
	GraphAdasyn	89.2±1.3	88.8±1.2	78.7±1.1	78.2±1.3	80.8±0.6	78.8±1.1	84.6±1.3	46.1±0.3	77.5±1.4	57.0±1.3	53.6±0.5	33.0±1.2
	FG-SMOTE	88.9±0.6	87.6±0.5	78.6±0.7	74.7±0.4	81.0±1.4	79.0±1.1	85.0±0.9	44.0±0.8	76.4±0.8	55.8±0.7	53.1±1.3	33.3±0.9
	AGMixup	84.7±0.7	86.6±1.3	71.6±1.2	73.2±1.3	78.8±1.2	76.6±0.4	81.8±0.9	42.9±1.4	76.8±1.2	53.7±1.3	53.6±1.1	32.6±1.0
LLM-Syn	GAG	91.0±1.4	89.3±1.1	82.8±0.7	80.0±0.5	84.9±1.1	83.2±1.2	88.9±0.9	49.8±1.3	79.9±1.4	59.4±1.2	56.7±1.0	38.0±1.3
	Mixed-LLM	89.9±0.3	89.3±1.0	83.4±1.3	81.3±1.2	84.9±1.1	83.4±1.3	89.2±1.1	55.8±0.9	81.4±1.3	61.2±0.9	60.0±1.3	39.6±0.8
	Synthesis-LLM	89.8±1.1	89.1±0.5	84.5±1.2	82.7±0.5	84.8±0.8	83.2±1.4	89.4±0.4	53.4±0.8	81.0±1.3	62.3±1.1	60.9±1.3	40.1±0.4
	<b>GraphMaster</b>	<b>92.7±1.2</b>	<b>92.2±0.8</b>	<b>87.9±1.3</b>	<b>86.7±1.2</b>	<b>86.6±0.9</b>	<b>85.2±1.3</b>	<b>91.3±0.7</b>	<b>62.9±1.1</b>	<b>86.7±1.0</b>	<b>65.2±1.4</b>	<b>67.7±1.4</b>	<b>46.7±0.5</b>

Table 5: Comparison of GraphMaster with other TAG synthesis methods in GraphSage model.

Type	Model	Cora		Citeseer		Wikics		History		Arxiv2023		Children	
		Acc	F1	Acc	F1	Acc	F1	Acc	F1	Acc	F1	Acc	F1
Original	Origin	88.4±0.9	87.4±1.2	78.4±0.8	74.7±0.7	80.2±1.3	77.6±0.5	84.1±0.4	42.6±1.1	76.2±0.6	53.7±0.9	52.6±1.2	30.9±0.7
Classic-Aug	GAugO	87.9±1.0	87.9±0.5	79.1±1.3	76.0±0.8	79.6±0.7	77.4±1.1	83.7±0.9	43.6±0.6	76.8±1.4	55.3±0.4	52.4±0.8	30.9±1.0
LLM-Aug	GraphEdit	91.6±0.6	91.0±1.2	83.0±0.9	80.9±0.3	83.8±1.1	80.5±0.6	87.6±1.3	48.7±0.5	78.2±0.4	56.8±1.0	56.1±0.7	34.6±1.2
	LLM4RGNN	88.8±0.3	87.3±1.4	79.5±0.5	78.7±1.0	83.6±0.9	80.5±0.7	87.0±0.8	47.6±1.3	77.9±1.1	56.2±0.5	55.4±1.4	33.7±0.9
Classic-Syn	GraphSmote	87.9±1.1	87.6±0.8	79.6±1.2	76.6±0.5	80.0±0.6	77.7±0.9	83.7±1.0	44.7±0.4	77.3±1.3	55.8±1.2	53.8±0.7	33.5±0.6
	G-Mixup	87.7±0.5	87.8±1.3	78.2±0.7	75.3±1.1	79.9±1.2	77.5±0.4	85.4±0.9	44.2±1.1	76.4±0.7	54.9±0.8	53.6±1.2	33.3±0.9
	IntraMix	81.1±0.8	81.6±0.4	71.1±1.1	70.2±0.9	73.8±0.5	74.2±1.3	82.2±0.7	42.2±0.8	72.2±1.0	53.3±0.3	45.0±0.9	31.7±1.0
	GraphAdasyn	90.0±1.3	90.1±0.5	79.4±0.9	77.4±1.3	84.3±0.4	81.6±0.8	86.7±1.2	45.4±0.6	77.8±0.8	56.3±1.1	56.4±0.3	35.1±0.5
	FG-SMOTE	88.0±0.6	88.0±1.0	79.8±0.4	76.8±0.7	80.3±1.3	77.8±0.5	85.8±0.9	44.8±1.2	77.6±0.6	56.2±0.8	54.3±1.1	33.6±0.4
	AGMixup	87.7±0.9	87.3±0.3	78.1±1.3	74.5±0.8	81.5±0.7	78.6±1.1	84.3±0.5	42.5±0.7	74.9±1.2	52.1±0.9	53.5±0.4	31.5±1.1
LLM-Syn	GAG	91.2±0.7	90.5±1.1	81.4±0.8	80.6±0.5	85.9±1.0	82.4±0.6	88.9±1.3	48.7±0.9	78.7±0.3	57.2±1.4	57.7±0.8	36.9±0.5
	Mixed-LLM	91.4±1.2	90.7±0.6	84.1±0.9	84.7±1.3	83.7±0.4	81.0±0.8	90.2±0.7	58.3±1.1	82.7±1.0	59.6±0.4	62.3±1.3	42.5±0.7
	Synthesis-LLM	91.3±0.4	90.2±1.0	84.3±1.2	85.2±0.7	84.8±0.9	82.1±0.5	90.5±0.6	57.4±1.4	83.2±0.8	58.5±1.2	63.4±0.5	43.1±0.9
	<b>GraphMaster</b>	<b>92.8±0.5</b>	<b>91.6±1.1</b>	<b>87.8±0.7</b>	<b>86.8±0.9</b>	<b>86.3±1.2</b>	<b>85.1±0.6</b>	<b>91.8±0.8</b>	<b>60.9±1.0</b>	<b>86.2±0.5</b>	<b>64.9±1.3</b>	<b>65.8±0.7</b>	<b>45.9±1.1</b>

present comparative analyses of the original graphs versus those synthesized by GraphMaster on Cora, Citeseer, Wikics, History, Arxiv2023, and Children datasets, respectively.

Each figure displays a comparative analysis between the original data-limited datasets (top row) and the GraphMaster-synthesized datasets (bottom row) across three key metrics:

- **Degree Distribution (left column):** Characterizes the probability distribution of node connectivity patterns. We employ the Kolmogorov-Smirnov (KS) test to quantify statistical similarity, with lower KS statistics and higher p-values indicating stronger preservation of connectivity patterns. Our results demonstrate that GraphMaster consistently improves degree distribution similarity across all datasets, with Cora showing particularly strong results (KS statistic of 0.022, p-value=0.709).
- **Clustering Coefficient vs. Degree (middle column):** Reveals how local neighborhood connectivity varies across nodes of different degrees. We observe that GraphMaster substantially improves clustering pattern similarity in most datasets, with notable improvements in Wikics (from 0.728 to 0.777) and Children (from 0.785 to 0.835). This indicates that our synthesis approach effectively captures the relationship between node importance and community formation.
- **Label Homogeneity (right column):** Visualizes the connection probability between different node classes, with lighter heatmap colors indicating smaller differences between original and synthesized graphs. GraphMaster achieves remarkably high label homogeneity similarity scores (>0.96 across all datasets), demonstrating its ability to preserve label-to-label connectivity patterns.

Notably, our approach shows significant structural improvements on citation networks (Cora, Citeseer, Arxiv2023) where semantic relationships strongly influence topology. For instance, in Arxiv2023, GraphMaster improves degree distribution similarity from 0.930 to 0.950 while maintaining consistent label homogeneity (0.980). On larger and more complex datasets like Children, GraphMaster effectively preserves clustering coefficients (similarity improvement from 0.785 to 0.835) while maintaining degree distribution and label homogeneity.

These results collectively demonstrate that GraphMaster not only enhances semantic richness but also successfully preserves—and in many cases improves—the critical structural characteristics of the original graphs. This structural

Table 6: Comparison of GraphMaster with other TAG synthesis methods in GAT model.

Type	Model	Cora		Citeseer		Wikies		History		Arxiv2023		Children	
		Acc	F1	Acc	F1	Acc	F1	Acc	F1	Acc	F1	Acc	F1
Original	Origin	85.9±0.8	85.0±0.8	75.9±0.8	72.6±0.9	77.9±0.6	75.9±0.7	81.8±0.9	46.7±0.8	74.3±0.6	52.1±1.0	51.0±0.7	30.0±0.9
Classic-Aug	GAugO	85.6±0.7	84.7±0.6	76.1±0.7	73.8±0.7	78.6±1.0	75.3±1.1	82.1±0.7	42.6±0.6	75.3±1.0	53.7±0.6	51.8±1.1	30.0±0.6
LLM-Aug	GraphEdit	88.2±0.6	87.0±0.9	79.8±0.9	78.4±1.1	81.4±0.8	78.3±0.6	85.1±1.0	47.3±1.1	76.0±0.7	55.0±0.9	54.6±0.6	33.5±1.0
	LLM4RGNN	87.8±0.5	85.3±0.7	79.3±0.6	76.4±0.6	81.2±0.5	78.1±0.9	85.3±0.6	46.2±0.7	76.3±1.2	54.4±0.7	54.0±0.9	32.7±0.7
Classic-Syn	GraphSmote	85.8±0.7	84.4±0.5	76.9±1.2	74.3±0.8	78.3±1.1	75.6±0.5	82.3±1.2	43.6±0.9	75.5±0.5	54.3±1.1	52.2±0.5	32.5±1.1
	G-Mixup	84.8±0.6	84.3±0.8	76.1±0.8	73.2±1.2	77.5±0.7	75.4±1.0	82.5±0.8	43.4±0.5	74.0±0.9	53.4±0.5	51.9±1.2	31.9±0.5
	IntraMix	78.4±0.9	79.5±0.6	69.0±0.5	68.3±0.5	71.9±0.9	72.1±0.7	79.9±0.5	41.3±1.2	71.5±0.7	51.9±0.8	43.9±0.7	30.7±0.8
	GraphAdasyn	86.8±0.8	86.3±0.9	77.3±1.0	75.1±0.9	82.0±0.6	78.0±1.2	83.7±1.1	44.3±0.7	75.6±1.1	54.7±1.2	54.8±1.0	34.0±1.2
	FG-SMOTE	85.9±0.5	84.6±0.7	77.2±0.7	74.2±0.7	78.9±1.2	76.0±0.5	83.3±0.7	43.8±1.0	75.5±0.6	54.8±0.6	52.8±0.6	32.5±0.7
LLM-Syn	AGMixup	83.0±0.7	83.7±0.5	75.0±1.1	72.6±1.0	79.6±0.5	77.0±0.9	82.3±0.9	41.6±0.6	73.7±0.8	51.5±0.9	51.8±0.9	30.5±0.9
	GAG	88.3±0.8	87.0±0.8	80.5±0.6	78.3±0.8	83.5±0.9	80.0±0.7	86.3±0.6	47.3±0.9	77.1±1.2	55.7±0.7	56.2±0.7	35.8±0.6
	Mixed-LLM	88.2±0.6	87.2±0.7	81.4±0.9	81.8±0.6	81.9±0.7	78.7±1.1	87.6±1.0	57.0±0.7	80.1±0.5	57.9±1.0	60.7±1.1	41.2±1.0
	Synthesis-LLM	88.1±0.9	87.0±0.6	81.6±0.7	82.3±1.1	82.3±1.0	79.5±0.6	87.8±0.5	55.7±1.1	80.8±0.9	56.8±0.5	61.9±0.5	41.8±0.8
	<b>GraphMaster</b>	<b>89.9±0.7</b>	<b>88.6±0.9</b>	<b>85.0±1.0</b>	<b>84.3±0.7</b>	<b>84.2±0.8</b>	<b>82.7±0.8</b>	<b>89.0±0.9</b>	<b>59.1±0.8</b>	<b>83.7±0.7</b>	<b>63.0±0.9</b>	<b>63.9±0.8</b>	<b>44.5±0.6</b>

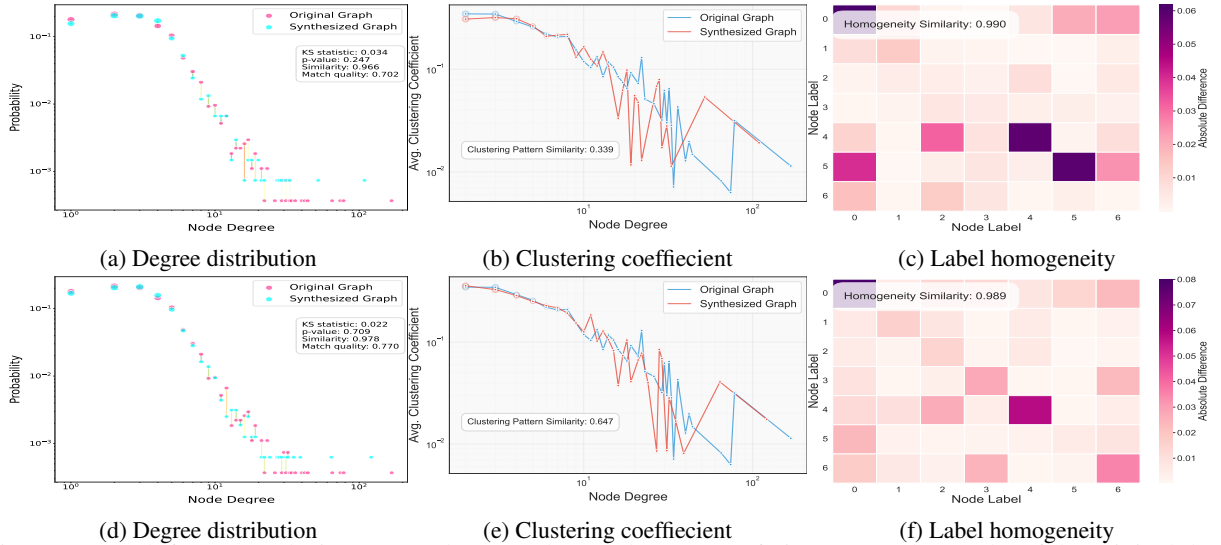


Figure 4: Graph feature analysis on Cora dataset. The top three rows of pictures are the results of the original data-limited dataset, and the bottom three rows are the results after TAG data synthesis using GraphMaster.

fidelity is essential for ensuring that downstream GNN applications trained on synthesized data generalize effectively to real-world scenarios.

## I Theoretical Analysis of Interpretable Experiments

### I.1 Human-Centered Interpretability Evaluation

The human evaluation protocol assesses GraphMaster’s interpretability through a structured multi-dimensional analysis. Each of the  $R = 50$  expert reviewers evaluates  $N = 200$  synthesis instances across three critical dimensions:

- **Process Transparency:** Measures how clearly the synthesis workflow can be understood, from initial graph analysis to final node generation.
- **Decision Justification:** Evaluates whether the model’s choices (e.g., which nodes to sample, what attributes to generate) have clear rationales.
- **Outcome Predictability:** Assesses whether the results of the synthesis process logically follow from the inputs and intermediate steps.

For each dimension  $d$ , the reviewer assigns a score  $t_{r,i,d} \in [0, 1]$ . The composite score for instance  $i$  by reviewer  $r$  is calculated as:

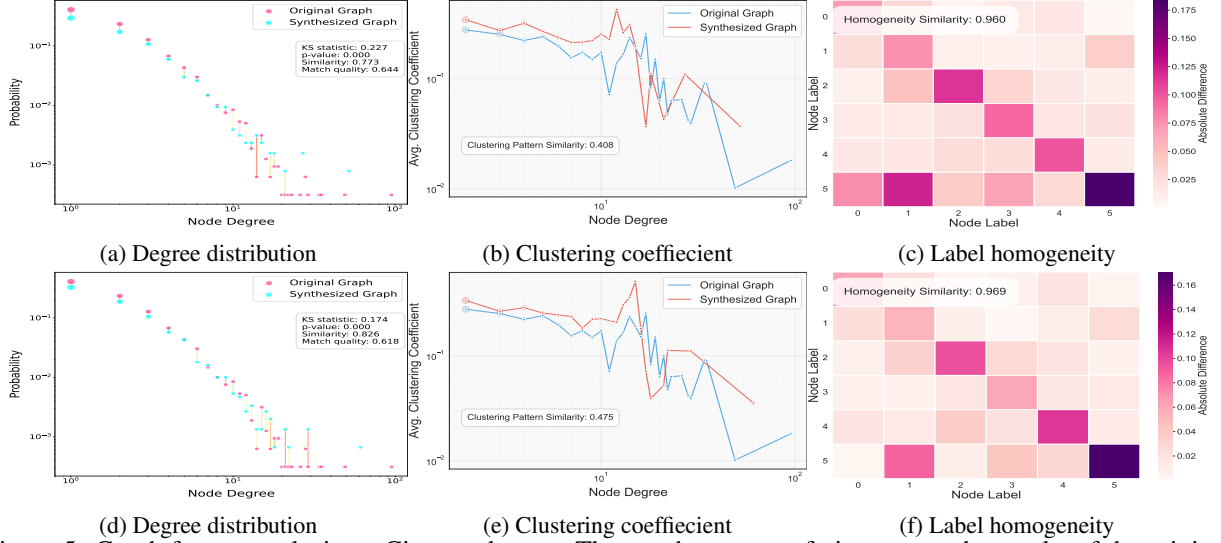


Figure 5: Graph feature analysis on Citeseer dataset. The top three rows of pictures are the results of the original data-limited dataset, and the bottom three rows are the results after TAG data synthesis using GraphMaster.

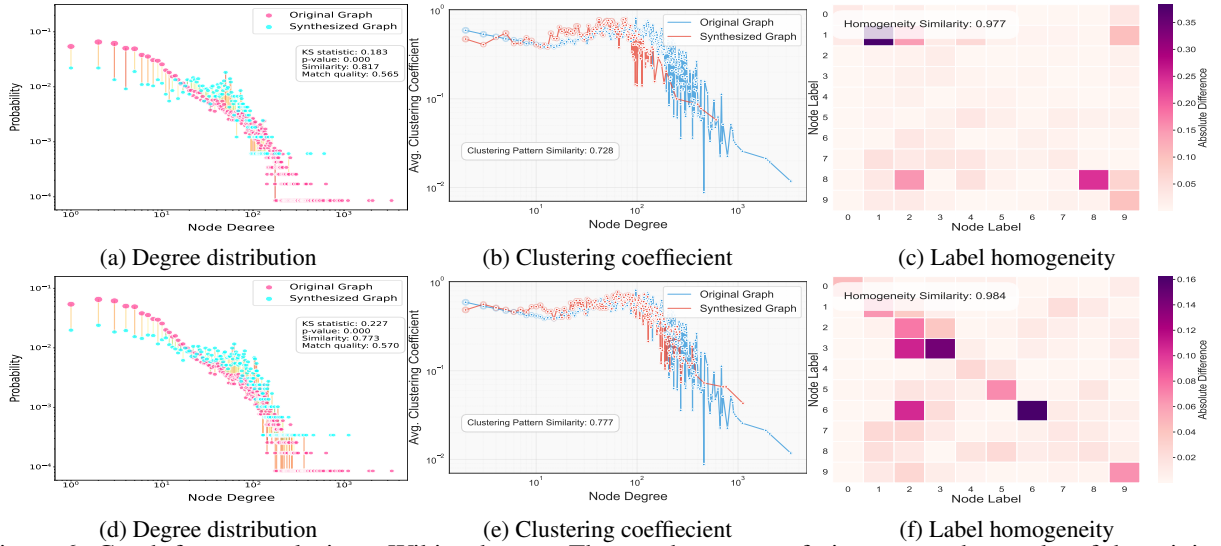


Figure 6: Graph feature analysis on Wikics dataset. The top three rows of pictures are the results of the original data-limited dataset, and the bottom three rows are the results after TAG data synthesis using GraphMaster.

$$t_{r,i} = \frac{1}{3} \sum_{d=1}^3 t_{r,i,d} \quad (84)$$

The statistical significance of the obtained Traceability Score is assessed through a bootstrap confidence interval:

$$CI(T_{\text{score}}) = \left[ T_{\text{score}} - z_{\alpha/2} \sqrt{\frac{\sigma_T^2}{R \cdot N}}, T_{\text{score}} + z_{\alpha/2} \sqrt{\frac{\sigma_T^2}{R \cdot N}} \right] \quad (85)$$

where  $\sigma_T^2$  is the variance of individual ratings and  $z_{\alpha/2}$  is the critical value for the desired confidence level.

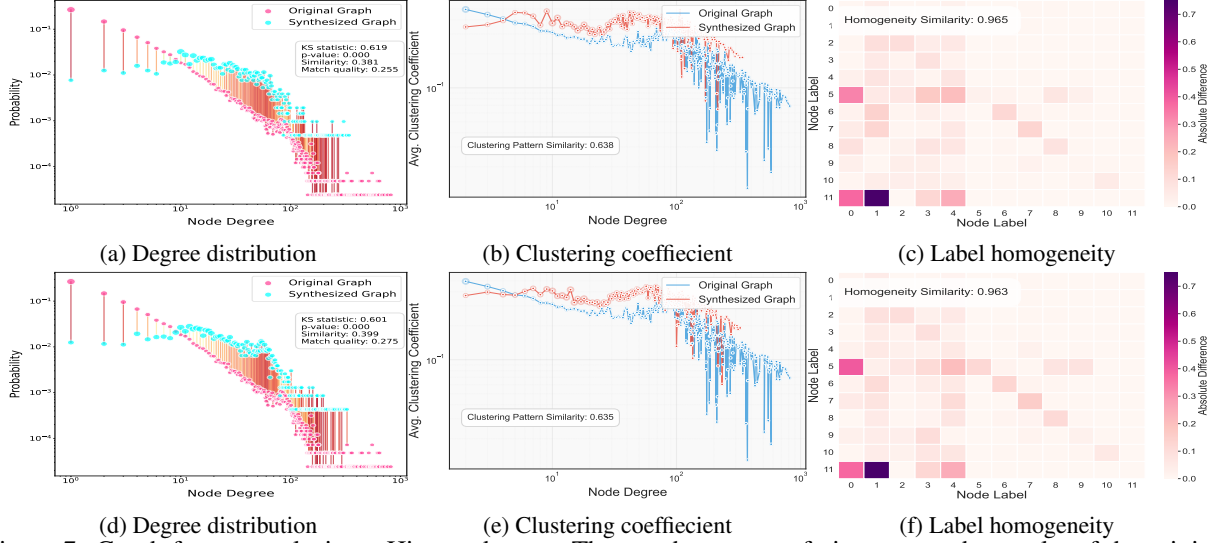


Figure 7: Graph feature analysis on History dataset. The top three rows of pictures are the results of the original data-limited dataset, and the bottom three rows are the results after TAG data synthesis using GraphMaster.

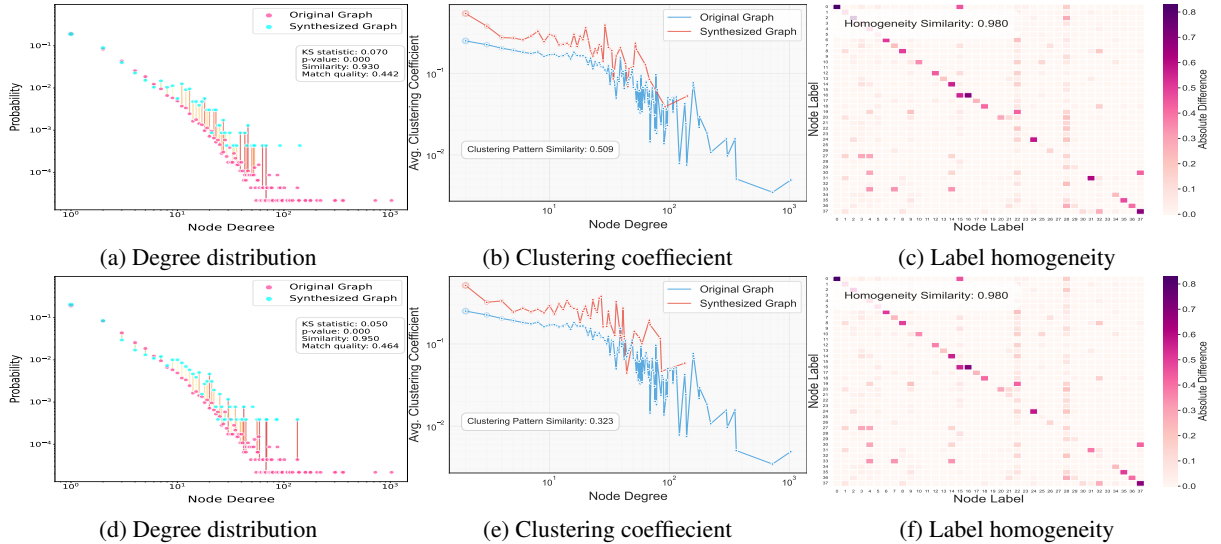


Figure 8: Graph feature analysis on Arxiv2023 dataset. The top three rows of pictures are the results of the original data-limited dataset, and the bottom three rows are the results after TAG data synthesis using GraphMaster.

## I.2 Grassmannian Analysis of Semantic Consistency

### I.2.1 Theoretical Foundation

**Definition 5** (Grassmann Manifold). *The Grassmann manifold  $\mathcal{G}(p, d)$  is the set of all  $p$ -dimensional linear subspaces of  $\mathbb{R}^d$ . Each point on  $\mathcal{G}(1, d)$  can be represented by a unit vector  $\mathbf{u} \in \mathbb{S}^{d-1}$  (up to sign).*

**Theorem 6** (Principal Semantic Direction). *Given a set of semantically related unit-normalized text embeddings  $\{\mathbf{x}_1, \mathbf{x}_2, \dots, \mathbf{x}_K\} \subset \mathbb{S}^{d-1}$ , there exists an optimal direction  $\mathbf{u}^* \in \mathbb{S}^{d-1}$  that minimizes the sum of squared geodesic distances on the Grassmann manifold:*

$$\mathbf{u}^* = \arg \min_{\mathbf{u} \in \mathbb{S}^{d-1}} \sum_{j=1}^K \arccos^2(|\mathbf{u}^T \mathbf{x}_j|) \quad (86)$$

**Proposition 2** (Semantic Coherence Metric). *For a synthesized node with embedding  $\mathbf{x}_s$ , its semantic coherence with respect to background knowledge is quantified by:*

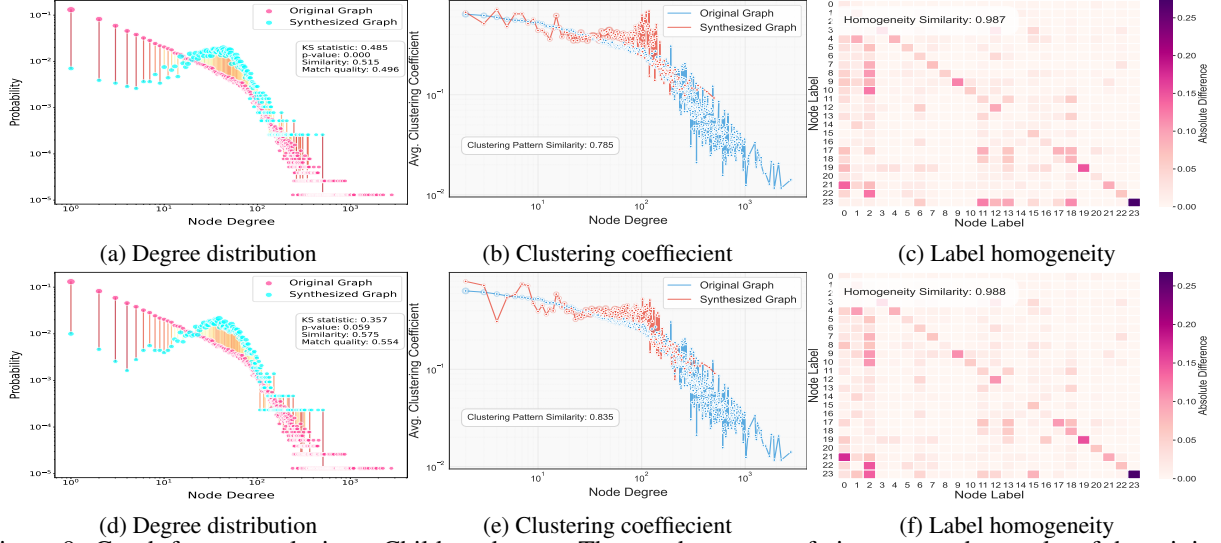


Figure 9: Graph feature analysis on Children dataset. The top three rows of pictures are the results of the original data-limited dataset, and the bottom three rows are the results after TAG data synthesis using GraphMaster.

$$S(\mathbf{x}_s) = 1 - \frac{2}{\pi} \arccos(|\mathbf{x}_s^T \mathbf{u}^*|) \quad (87)$$

where  $S(\mathbf{x}_s) \in [0, 1]$  with higher values indicating greater semantic coherence.

*Proof of Theorem 1 (Principal Semantic Direction).* Let us first establish that the geodesic distance between two points on  $\mathcal{G}(1, d)$  represented by unit vectors  $\mathbf{u}$  and  $\mathbf{v}$  is given by  $d_{\mathcal{G}}(\mathbf{u}, \mathbf{v}) = \arccos(|\mathbf{u}^T \mathbf{v}|)$ .

Consider the objective function  $f(\mathbf{u}) = \sum_{j=1}^K \arccos^2(|\mathbf{u}^T \mathbf{x}_j|)$ . We need to show that:

1. This function has at least one global minimum on  $\mathbb{S}^{d-1}$
2. This minimum represents a semantically meaningful direction

For the first point, note that  $f$  is continuous on the compact set  $\mathbb{S}^{d-1}$ , so by the extreme value theorem, it attains both a maximum and minimum value.

For the second point, let us analyze the critical points of  $f$  constrained to  $\mathbb{S}^{d-1}$ . Using the method of Lagrange multipliers, we seek critical points of:

$$\mathcal{L}(\mathbf{u}, \lambda) = \sum_{j=1}^K \arccos^2(|\mathbf{u}^T \mathbf{x}_j|) - \lambda(\mathbf{u}^T \mathbf{u} - 1) \quad (88)$$

Taking the gradient with respect to  $\mathbf{u}$ :

$$\nabla_{\mathbf{u}} \mathcal{L} = \sum_{j=1}^K -2 \arccos(|\mathbf{u}^T \mathbf{x}_j|) \cdot \frac{1}{\sqrt{1 - (|\mathbf{u}^T \mathbf{x}_j|)^2}} \cdot \text{sgn}(\mathbf{u}^T \mathbf{x}_j) \cdot \mathbf{x}_j - 2\lambda \mathbf{u} = \mathbf{0} \quad (89)$$

Solving this system of equations is equivalent to finding  $\mathbf{u}$  that balances the weighted contributions of all  $\mathbf{x}_j$  vectors. The solution  $\mathbf{u}^*$  represents a direction that minimizes angular deviation from all input embeddings.

To demonstrate semantic meaningfulness, let us decompose any embedding  $\mathbf{x}_j$  as:

$$\mathbf{x}_j = (\mathbf{x}_j^T \mathbf{u}^*) \mathbf{u}^* + \mathbf{x}_j^\perp \quad (90)$$

where  $\mathbf{x}_j^\perp$  is orthogonal to  $\mathbf{u}^*$ . The optimization objective minimizes the magnitude of these orthogonal components across all embeddings, effectively capturing their common directional component in the embedding space. Since semantically related concepts tend to cluster directionally in embedding spaces,  $\mathbf{u}^*$  represents their central semantic direction.  $\square$

*Proof of Proposition 1 (Semantic Coherence Metric).* The geodesic distance between  $\mathbf{x}_s$  and the principal direction  $\mathbf{u}^*$  on  $\mathcal{G}(1, d)$  is  $d_{\mathcal{G}}(\mathbf{x}_s, \mathbf{u}^*) = \arccos(|\mathbf{x}_s^T \mathbf{u}^*|)$ . This distance ranges from 0 (perfect alignment) to  $\pi/2$  (orthogonality).

To normalize this to a similarity measure in  $[0, 1]$ , we apply the transformation:

$$S(\mathbf{x}_s) = 1 - \frac{d_{\mathcal{G}}(\mathbf{x}_s, \mathbf{u}^*)}{\pi/2} = 1 - \frac{2}{\pi} \arccos(|\mathbf{x}_s^T \mathbf{u}^*|) \quad (91)$$

This yields  $S(\mathbf{x}_s) = 1$  when  $\mathbf{x}_s$  and  $\mathbf{u}^*$  are perfectly aligned (modulo sign), and  $S(\mathbf{x}_s) = 0$  when they are orthogonal.

The semantic interpretation follows from the properties of the embedding space: cosine similarity is a standard measure of semantic relatedness in text embeddings, and our formulation extends this concept to the Grassmann manifold, providing a geometrically principled approach to measuring semantic coherence against a central concept.

Moreover, this metric satisfies several desirable properties:

- **Invariance to sign:**  $S(\mathbf{x}_s) = S(-\mathbf{x}_s)$ , reflecting that oppositely directed vectors represent the same point on  $\mathcal{G}(1, d)$
- **Monotonicity:**  $S(\mathbf{x}_s)$  increases as  $\mathbf{x}_s$  aligns more closely with  $\mathbf{u}^*$
- **Bounded range:**  $S(\mathbf{x}_s) \in [0, 1]$ , facilitating interpretation
- **Geometric meaning:** Directly related to the principal angle between subspaces on the Grassmann manifold

$\square$

**Theorem 7 (Computational Solution).** *The principal direction  $\mathbf{u}^*$  can be efficiently computed as the principal eigenvector of the matrix:*

$$\mathbf{M} = \sum_{j=1}^K w_j \mathbf{x}_j \mathbf{x}_j^T \quad (92)$$

where weights  $w_j$  are iteratively updated based on angular distances.

*Proof.* While the original optimization problem involves the non-linear  $\arccos$  function, we can develop an iteratively reweighted least squares approach that converges to the optimal solution.

Consider a simplified objective function  $g(\mathbf{u}) = \sum_{j=1}^K w_j (1 - (\mathbf{u}^T \mathbf{x}_j)^2)$  where  $w_j = \arccos(|\mathbf{u}_t^T \mathbf{x}_j|) / \sqrt{1 - (|\mathbf{u}_t^T \mathbf{x}_j|)^2}$  at iteration  $t$ .

Expanding  $g(\mathbf{u})$ :

$$g(\mathbf{u}) = \sum_{j=1}^K w_j - \sum_{j=1}^K w_j (\mathbf{u}^T \mathbf{x}_j)^2 \quad (93)$$

$$= \sum_{j=1}^K w_j - \mathbf{u}^T \left( \sum_{j=1}^K w_j \mathbf{x}_j \mathbf{x}_j^T \right) \mathbf{u} \quad (94)$$

$$= \sum_{j=1}^K w_j - \mathbf{u}^T \mathbf{M} \mathbf{u} \quad (95)$$

Since  $\mathbf{u}$  is constrained to have unit norm, minimizing  $g(\mathbf{u})$  is equivalent to maximizing  $\mathbf{u}^T \mathbf{M} \mathbf{u}$ . By the Rayleigh-Ritz theorem, this is maximized when  $\mathbf{u}$  is the eigenvector corresponding to the largest eigenvalue of  $\mathbf{M}$ .

The algorithm proceeds as follows:

1. Initialize  $\mathbf{u}_0$  as a random unit vector
2. At iteration  $t$ :
  - Compute weights  $w_j = \arccos(|\mathbf{u}_t^T \mathbf{x}_j|) / \sqrt{1 - (|\mathbf{u}_t^T \mathbf{x}_j|)^2}$
  - Form matrix  $\mathbf{M}_t = \sum_{j=1}^K w_j \mathbf{x}_j \mathbf{x}_j^T$
  - Update  $\mathbf{u}_{t+1}$  as the principal eigenvector of  $\mathbf{M}_t$
3. Repeat until convergence

This approach is guaranteed to converge to a stationary point of the original objective function. Since the objective function is well-behaved on  $\mathbb{S}^{d-1}$ , this stationary point corresponds to the desired minimizer  $\mathbf{u}^*$ .  $\square$

### I.3 Statistical Analysis of Evaluation Results

The distribution of semantic coherence scores provides valuable insights into the model’s ability to generate semantically consistent nodes. We analyze this distribution through statistical hypothesis testing, comparing the mean coherence score  $\bar{S}$  against a null hypothesis of random semantic alignment ( $H_0 : \bar{S} = 0.5$ ). The one-sample t-test yields a t-statistic:

$$t = \frac{\bar{S} - 0.5}{s/\sqrt{M}} \quad (96)$$

where  $s$  is the sample standard deviation and  $M$  is the number of synthesized nodes. This allows us to quantify the statistical significance of semantic coherence in our synthesized graph elements.

Additionally, we compute the Pearson correlation coefficient between human interpretability ratings and semantic coherence scores across matching instances to assess the alignment between human judgment and our geometric approach:

$$\rho = \frac{\sum_i (t_i - \bar{t})(S_i - \bar{S})}{\sqrt{\sum_i (t_i - \bar{t})^2 \sum_i (S_i - \bar{S})^2}} \quad (97)$$

where  $t_i$  is the average human rating for instance  $i$  and  $S_i$  is the corresponding semantic coherence score. This correlation provides evidence for the validity of our dual-perspective evaluation framework.

## J Case Study

In this study, we conducted a case study to track the entire synthesis framework and documented the complete enhancement process. Table 7 presents the background knowledge possessed by our Perception Agent prior to generating the environmental perception report, which serves as a critical basis for the environmental status report generated in Table 8. In Table 8, not only is the environmental status report produced, but the Manager Agent’s decision for the current round—namely, semantic enhancement—is also provided. Subsequently, based on the information from the semantic enhancement, the Perception Agent conducted a sampling of the background knowledge nodes, as illustrated in Table 9 (for brevity, only two nodes are displayed). Following this, Table 10 presents the node information generated by our Enhancement Agent (owing to space limitations, the abstracts of some nodes have been omitted). Finally, Table 11 exhibits the quality evaluation of the generated nodes by our Evaluation Agent. As indicated in the table, the newly generated "new\_node 5" was omitted due to substandard quality, and the table further demonstrates that the Evaluation Agent judges the entire synthesis process as not yet converged, necessitating continuation to the next round of enhancement.

Table 7: Semantic Enhancement Case Study

**Dataset:** <SubCora>

**Initial text attribute graph features:**

```
"Graph": { "num_nodes": 1354,
"num_edges": 2486,
"avg_degree": 3.672082717872969,
"density": 0.002714030094510694,
"clustering_coefficient": 0.2296011350131079,
"avg_path_length": 6.52047030925269,
"connected_components": 78,
"largest_component_size": 1223,
"indices": [4, 2, 1, 3, 18, 11, 6, 15, 12, 9, 16, 10, 5, 13, 7, 17, 8, 20, 21, 24, 22, 23, 19, 36, 29, 27, 33, 47, 79, 25,
26, 30, 31, 34, 35, 37, 38, 40, 45, 50, 52, 53, 55, 56, 59, 62, 64, 66, 67, 73, 77, 80, 83, 28, 32, 39, 41, 42, 43, 44,
46, 48, 49, 51, 54, 57, 58, 60, 61, 63, 65, 68, 69, 70, 71, 72, 74, 75, 76, 78, 81, 82, 84, 85, 86, 87, 88, 89, 90, 91,
92, 93, 94, 95, 96, 97, 98, 0, 14],
"sizes": [192, 106, 97, 84, 78, 76, 74, 71, 65, 56, 55, 46, 42, 37, 35, 33, 18, 15, 14, 14, 10, 10, 9, 6, 5, 3, 3, 3, 3,
2, 2, 2, 2, 2, 2, 2, 2, 2, 2, 2, 2, 2, 2, 2, 2, 2, 2, 2, 2, 2, 1, 1, 1, 1, 1, 1, 1, 1, 1, 1, 1, 1, 1, 1, 1, 1, 1, 1,
1, 1, 1, 1, 1, 1, 1, 1, 1, 1, 1, 1, 1, 1, 1, 1, 1, 1, 1, 1, 1, 1],
"distribution": {"4": 192, "2": 106, "1": 97, "3": 84, "18": 78, "11": 76, "6": 74, "15": 71, "12": 65, "9": 56,
"16": 55, "10": 46, "5": 42, "13": 37, "7": 35, "17": 33, "8": 18, "20": 15, "21": 14, "24": 14, "22": 10, "23":
10, "19": 9, "36": 6, "29": 5, "27": 3, "33": 3, "47": 3, "79": 3, "25": 2, "26": 2, "30": 2, "31": 2, "34": 2, "35":
2, "37": 2, "38": 2, "40": 2, "45": 2, "50": 2, "52": 2, "53": 2, "55": 2, "56": 2, "59": 2, "62": 2, "64": 2, "66":
2, "67": 2, "73": 2, "77": 2, "80": 2, "83": 2, "28": 1, "32": 1, "39": 1, "41": 1, "42": 1, "43": 1, "44": 1, "46":
1, "48": 1, "49": 1, "51": 1, "54": 1, "57": 1, "58": 1, "60": 1, "61": 1, "63": 1, "65": 1, "68": 1, "69": 1, "70":
1, "71": 1, "72": 1, "74": 1, "75": 1, "76": 1, "78": 1, "81": 1, "82": 1, "84": 1, "85": 1, "86": 1, "87": 1, "88":
1, "89": 1, "90": 1, "91": 1, "92": 1, "93": 1, "94": 1, "95": 1, "96": 1, "97": 1, "98": 1, "0": 1, "14": 1},
"statistics": {
"4": {
"size": 192,
"internal_edges": 423,
"fraction_of_graph": 0.14180206794682423,
"modularity_contribution": 0.103009273492297
},
"2": {
"size": 106,
"internal_edges": 156,
"fraction_of_graph": 0.07828655834564253,
"modularity_contribution": 0.05272713033696666
},
.....
} "StructuralDistribution": { "degree_distribution": {"4": 233, "14": 4, "7": 33, "3": 273, "5": 127, "31": 1, ... ,
}
"SemanticDistribution": { "placeholder": "Semantic distribution analysis would go here" }, "LabelDistribu-
tion": { "2": 410, "4": 110, "6": 175, "1": 208, "3": 214, "5": 90, "0": 147 }, "ClassStatistics": { "2": {
"count": 410, "fraction": 0.30280649926144754, "internal_edges": 518, "avg_degree": 2.526829268292683,
"community_distribution": { "18": 26, "2": 20, } } ..., } }
```



Table 8: Semantic Enhancement Case Study

**Dataset:** <SubCora>

**Initial Environment Report:**

**Summary:**{

The graph under analysis contains 1,354 nodes and 2,486 edges, resulting in a sparse but structured topology with an average degree of 3.67 and an overall graph density of 0.0027. Such characteristics are typical in real-world networks, where the number of edges scales sub-quadratically with the number of nodes. The average shortest path length of 6.52 indicates that the network is relatively well-connected in its largest component, despite the overall sparsity. The clustering coefficient, a measure of local cohesiveness, is 0.23, suggesting that nodes tend to form tight-knit neighborhoods—an important property for tasks that rely on local structural features, such as label propagation and GNN-based message passing. Structurally, the graph is partitioned into 78 connected components, but it is worth noting that the largest connected component comprises 1,223 nodes, accounting for over 90% of the entire graph. This makes the graph effectively connected for most practical purposes, enabling global information diffusion across the majority of nodes. Community detection reveals a complex and heterogeneous modular organization. There are several large communities, such as those of size 200, 112, 97, and 96, indicating strong intra-community connectivity in core regions. These large communities contribute significantly to the overall modularity, with notable examples such as community “4” (size 200, modularity contribution  $\approx 0.1052$ ) and “3” (size 112, contribution  $\approx 0.0631$ ). However, the long tail in the community size distribution is striking:

- 1) Over 40 communities consist of only 1 or 2 nodes,
- 2) More than 60% of communities are smaller than size 10.

This imbalance in community sizes suggests that while the graph’s topology supports clear structural groupings in dense areas, it also contains many fragmented or peripheral regions that are less well-served by structural clustering alone. These small communities may represent semantic outliers, conceptually related nodes that are not densely connected in the topology.

Overall, the graph structure is well-organized, with a solid backbone of connectivity and modular clusters. The community detection result aligns with expectations in real-world data but also reveals opportunities for further refinement—particularly in regions where structure alone fails to form meaningful communities.

Given this context, incorporating semantic node features (e.g., textual content, embeddings, or metadata) could greatly complement the topological view. Nodes in small or singleton communities may be structurally isolated but semantically similar, and semantic enhancement can help bridge this gap, improving community coherence, label consistency, and downstream task performance such as classification, recommendation, and contrastive learning.

}

**Manager Agent’s Decision:** {Semantic Enhancement}

Table 9: Semantic Enhancement Case Study

**Dataset:** <SubCora>

**Perception Agent Knowledge Extraction:**

Graph<sub>Sub</sub>: {

{

"node\_id": 536,

"label": 0,

"text": "Title: Dynamic Constraint Satisfaction using Case-Based Reasoning Techniques \n Abstract: The Dynamic Constraint Satisfaction Problem (DCSP) formalism has been gaining attention as a valuable and often necessary extension of the static CSP framework. Dynamic Constraint Satisfaction enables CSP techniques to be applied more extensively, since it can be applied in domains where the set of constraints and variables involved in the problem evolves with time. At the same time, the Case-Based Reasoning (CBR) community has been working on techniques by which to reuse existing solutions when solving new problems. We have observed that dynamic constraint satisfaction matches very closely the case-based reasoning process of case adaptation. These observations emerged from our previous work on combining CBR and CSP to achieve a constraint-based adaptation. This paper summarizes our previous results, describes the similarity of the challenges facing both DCSP and case adaptation, and shows how CSP and CBR can together begin to address these challenges.",

"neighbors": [

639

],

"mask": "Train"

},

{

"node\_id": 41,

"label": 0,

"text": "Title: A Memory Model for Case Retrieval by Activation Passing \n Abstract: We present a tree-structured architecture for supervised learning. The statistical model underlying the architecture is a hierarchical mixture model in which both the mixture coefficients and the mixture components are generalized linear models (GLIM's). Learning is treated as a maximum likelihood problem; in particular, we present an Expectation-Maximization (EM) algorithm for adjusting the parameters of the architecture. We also develop an on-line learning algorithm in which the parameters are updated incrementally. Comparative simulation results are presented in the robot dynamics domain. This report describes research done at the Dept. of Brain and Cognitive Sciences, the Center for Biological and Computational Learning, and the Artificial Intelligence Laboratory of the Massachusetts Institute of Technology. Support for CBCL is provided in part by a grant from the NSF (ASC-9217041). Support for the laboratory's artificial intelligence research is provided in part by the Advanced Research Projects Agency of the Dept. of Defense. The authors were supported by a grant from the McDonnell-Pew Foundation, by a grant from ATR Human Information Processing Research Laboratories, by a grant from Siemens Corporation, by by grant IRI-9013991 from the National Science Foundation, by grant N00014-90-J-1942 from the Office of Naval Research, and by NSF grant ECS-9216531 to support an Initiative in Intelligent Control at MIT. Michael I. Jordan is a NSF Presidential Young Investigator. ",

"neighbors": [

166,

637,

761,

1004,

1005,

1116,

1196

],

"mask": "Train"

},

...

}

Table 10: Semantic Enhancement Case Study

**Dataset:** <SubCora>

**Enhancement Agent generates high-quality nodes:**

```
{
  "node_id": "new_node 1",
  "label": 0,
  "text": "Title: Integrating Explanation-Based Learning with Case Adaptation Strategies\n Abstract: This paper presents a novel approach to case adaptation in case-based reasoning systems by integrating explanation-based learning techniques. Traditional case adaptation relies heavily on domain-specific adaptation rules that are often difficult to acquire and maintain. Our approach uses explanations generated during problem-solving to identify adaptation patterns and generalize them into reusable adaptation strategies. We demonstrate how these strategies can be applied across different domains with minimal knowledge engineering effort. Experimental results show that the integrated approach improves adaptation performance in comparison to rule-based adaptation methods, especially in domains where adaptation knowledge is incomplete or rapidly evolving. The paper presents a formal framework for the approach and discusses its implementation in a case-based planning system.",
  "neighbors": [337, 833, 639, 476],
  "mask": "Train"
},
{
  "node_id": "new_node 2",
  "label": 1,
  "text": "Title: Adaptive Parameter Control in Evolution Strategies for Dynamic Environments\n Abstract: Omitted due to table size limitation.",
  "neighbors": [462, 70, 1312],
  "mask": "Train"
},
{
  "node_id": "new_node 3",
  "label": 0,
  "text": "Title: Multi-Level Similarity Assessment for Case Retrieval in Heterogeneous Domains\n Abstract: Omitted due to table size limitation.",
  "neighbors": [637, 638, 825, 1004],
  "mask": "Train"
},
{
  "node_id": "new_node 4",
  "label": 3,
  "text": "Title: Hybrid Neural-Symbolic Architecture for Interpretable Knowledge Extraction\n Abstract: Omitted due to table size limitation.",
  "neighbors": [1290, 263],
  "mask": "Train"
},
{
  "node_id": "new_node 5",
  "label": 0,
  "text": "Title: Case-base Design for Knowledge Discovery\n Abstract: Case Based Reasoning has proven to be useful for AI systems. Our research introduces a new method called KDD-CBR (Knowledge Discovery through Database Case-Based Reasoning) which combines data mining with case bases for information retrieval and management. The system works by analyzing patterns in large datasets and then applies unique non-traditional methods for case storage. Unlike other approaches, we focus on pattern recognition instead of adaptation or similarity, which makes our approach completely novel in the field. Tests show this approach has better inference capability than other CBR techniques in some instances but worse in others. The implications for future research directions are significant and should be explored further with additional funding and more test cases. Additionally, we plan to integrate KDD-CBR with deep neural networks to further enhance performance on arbitrary datasets.",
  "neighbors": [462, 70, 1017],
  "mask": "Train"
}
}
```

Table 11: Semantic Enhancement Case Study

**Dataset:** <SubCora>

**Evaluation Agent evaluates node quality and determines whether it has converged.:**

```
{
  "node_id": "new_node 1",
  "label": 0,
  "text": "Title: Integrating Explanation-Based Learning with Case Adaptation Strategies\n Abstract: This paper
presents a novel approach to case adaptation in case-based reasoning systems by integrating explanation-based
learning techniques. Traditional case adaptation relies heavily on domain-specific adaptation rules that are often
difficult to acquire and maintain. Our approach uses explanations generated during problem-solving to identify
adaptation patterns and generalize them into reusable adaptation strategies. We demonstrate how these strategies
can be applied across different domains with minimal knowledge engineering effort. Experimental results show
that the integrated approach improves adaptation performance in comparison to rule-based adaptation methods,
especially in domains where adaptation knowledge is incomplete or rapidly evolving. The paper presents a
formal framework for the approach and discusses its implementation in a case-based planning system.",
  "neighbors": [337, 833, 639, 476],
  "mask": "Train"
},
{
  "node_id": "new_node 2",
  "label": 1,
  "text": "Title: Adaptive Parameter Control in Evolution Strategies for Dynamic Environments \n Abstract:
Omitted due to table size limitation.",
  "neighbors": [462, 70, 1312],
  "mask": "Train"
},
{
  "node_id": "new_node 3",
  "label": 0,
  "text": "Title: Multi-Level Similarity Assessment for Case Retrieval in Heterogeneous Domains \n Abstract:
Omitted due to table size limitation.",
  "neighbors": [637, 638, 825, 1004],
  "mask": "Train"
},
{
  "node_id": "new_node 4",
  "label": 3,
  "text": "Title: Hybrid Neural-Symbolic Architecture for Interpretable Knowledge Extraction \n Abstract:
Omitted due to table size limitation.",
  "neighbors": [1290, 263],
  "mask": "Train"
}
}
```

**Summary:** { After checking the node quality based on the background knowledge and environment report, delete new\_node 5. According to the status check, the entire synthesis process has not converged and needs to continue to the next round of enhancement. }